REPORT 1250

THE DYNAMIC-RESPONSE CHARACTERISTICS OF A 35° SWEPT-WING AIRPLANE AS DETERMINED FROM FLIGHT MEASUREMENTS [1]

By William C. Triplett, Stuart C. Brown, and G. Allan Smith

SUMMARY

The longitudinal and lateral-directional dynamic-response characteristics of a 35° swept-wing fighter-type airplane determined from flight measurements are presented and compared with predictions based on theoretical studies and wind-tunnel data. Flights were made at an altitude of 35,000 feet covering the Mach number range of 0.50 to 1.04. A limited amount of lateral-directional data were also obtained at 10,000 feet. The flights consisted essentially of recording transient responses to pilot-applied pulsed motions of each of the three primary control surfaces. These transient data were converted into frequency-response form by means of the Fourier transformation and compared with predicted responses calculated from the basic equations of motion. The equations, or transfer functions, that best describe the various measured responses were evaluated by a curve-fitting process involving the use of templates and an analog computer. By this method it was generally possible to find equations, of simple form, that closely matched the experimental frequency responses between 1 and 10 radians per second and at the same time adequately described the recorded time histories.

Experimentally determined transfer functions were used for the evaluation of the stability derivatives that have the greatest effect on the dynamic response of the airplane. The values of these derivatives, in most cases, agreed favorably with predictions over the Mach number range of the test.

INTRODUCTION

In the design of automatic-control equipment for high performance aircraft, the dynamic response characteristics of the aircraft must be considered. It is desirable to express these characteristics as transfer functions which are expressions that describe the motion of the airplane for the various flight conditions of interest. The airplane can then be represented as a single element in a more complex closed-loop system.

Often these dynamic characteristics can be predicted by using stability derivatives obtained from wind-tunnel tests. In many cases, however, particularly in the transonic speed range, flight-test procedures are desirable to document the dynamic behavior of the airplane. Flight tests also serve the additional purpose of enabling comparisons to be made with predicted results, thus aiding in the development of more refined prediction methods.

This report describes the results of a flight investigation in which the dynamic-response characteristics of a 35° swept-wing airplane have been evaluated through the Mach number range of 0.50 to 1.04. Responses to transient rather than sinusoidal control inputs have been chosen for analysis because of convenience in making flight measurements. Certain useful information can be obtained directly from data recorded in transient-time-history form; however, when converted to frequency response form, the dynamic response of the aircraft is presented in a standard manner independent of the particular input used, and the dynamic characteristics are more readily apparent. The frequency-response data are also applicable to analysis by conventional servomechanism methods.

Experimental frequency responses will be described by analytical expressions termed "transfer functions" which are evaluated by a method utilizing a set of frequency-response templates and an analog computer. Whenever possible, the coefficients of these transfer functions are expressed in conventional stability-derivative form and compared with wind-tunnel and theoretical estimates.

NOTATION

C_L	lift coefficient
C_l	rolling-moment coefficient
C_m	pitching-moment coefficient
C_n	yawing-moment coefficient
C_Y	side-force coefficient
D	the operator, $\frac{d}{dt}$
I_X, I_Y, I_Z	moments of inertia about the X, Y, and Z axes, slug-ft^2
I_{XZ}	product of inertia, slug-ft^2
M	Mach number
R, I	real and imaginary parts of a complex quantity
S	wing area, sq ft
V	velocity, ft/sec
W	weight of airplane, lb
b	wing span, ft
c	mean aerodynamic chord, ft
g	acceleration due to gravity, ft/sec^2
i	$\sqrt{-1}$
m	mass of airplane, slugs
n	normal acceleration, $V(\dot{\alpha}-g)$, ft/sec^2 (except as noted)

[1] Supersedes recently declassified NACA RM A51G27 by William C. Triplett and G. Allan Smith, and NACA RM A52I17 by William C. Triplett and Stuart C. Brown.

p	rolling velocity, radians/sec
q	pitching velocity, radians/sec
$\dot{q}$	$\frac{dq}{dt}$, radians/sec^2
q_o	dynamic pressure, lb/sq ft
r	yawing velocity, radians/sec
t	time, sec
α	angle of attack, radians (except as noted)
$\dot{\alpha}$	$\frac{d\alpha}{dt}$, radians/sec
β	sideslip angle, radians (except as noted)
γ	flight-path angle, deg
δ	control deflection, radians (except as noted)
δ_a	total aileron deflection, radians (except as noted)
δ_e	elevator deflection, radians (except as noted)
δ_r	rudder deflection, radians (except as noted)
ζ	damping ratio
λ	root of the characteristic equation
σ	real part of a complex root
φ	angle of bank, radians
Φ	phase angle, deg
ψ	angle of yaw, radians
ω	frequency, radians/sec
ω_1	natural frequency of oscillation, radians/sec
ω_n	undamped natural frequency, radians/sec
C_{l_p}	$\frac{\partial C_l}{\partial(pb/2V)}$, per radian
C_{l_r}	$\frac{\partial C_l}{\partial(rb/2V)}$, per radian
C_{l_β}	$\frac{\partial C_l}{\partial\beta}$, per radian
C_{n_p}	$\frac{\partial C_n}{\partial(pb/2V)}$, per radian
C_{n_r}	$\frac{\partial C_n}{\partial(rb/2V)}$, per radian
C_{n_β}	$\frac{\partial C_n}{\partial\beta}$, per radian
C_{Y_β}	$\frac{\partial C_Y}{\partial\beta}$, per radian
C_{l_δ}	$\frac{\partial C_l}{\partial\delta}$, per radian
C_{n_δ}	$\frac{\partial C_n}{\partial\delta}$, per radian
C_{L_α}	$\frac{dC_L}{d\alpha}$, per radian
$C_{L_{\delta_e}}$	$\frac{dC_L}{d\delta_e}$, per radian
C_{m_α}	$\frac{dC_m}{d\alpha}$, per radian
$C_{m_{\delta_e}}$	$\frac{dC_m}{d\delta_e}$, per radian
C_{m_q}	$\frac{dC_m}{d(qc/2V)}$, per radian
$C_{m_{\dot{\alpha}}}$	$\frac{dC_m}{d(\dot{\alpha}c/2V)}$, per radian
C_{Y_δ}	$\frac{\partial C_Y}{\partial\delta}$, per radian
L_p	$\frac{q_o S b^2}{2VI_X} C_{l_p}$, per sec
L_r	$\frac{q_o S b^2}{2VI_X} C_{l_r}$, per sec
L_β	$\frac{q_o S b}{I_X} C_{l_\beta}$, per sec^2
M_α	$\frac{q_o S c}{I_Y} C_{m_\alpha}$, per sec^2
$M_{\dot{\alpha}}$	$\frac{q_o S c^2}{2VI_Y} C_{m_{\dot{\alpha}}}$, per sec
M_q	$\frac{q_o S c^2}{2VI_Y} C_{m_q}$, per sec
N_p	$\frac{q_o S b^2}{2VI_Z} C_{n_p}$, per sec
N_r	$\frac{q_o S b^2}{2VI_Z} C_{n_r}$, per sec
N_β	$\frac{q_o S b}{I_Z} C_{n_\beta}$, per sec^2
Y_β	$\frac{q_o S}{mV} C_{Y_\beta}$, per sec
L_δ	$\frac{q_o S b}{I_X} C_{l_\delta}$, per sec^2
N_δ	$\frac{q_o S b}{I_Z} C_{n_\delta}$, per sec^2
Y_δ	$\frac{q_o S}{mV} C_{Y_\delta}$, per sec
Z_α	$-\frac{q_o S}{mV} C_{L_\alpha}$, per sec
Z_δ	$-\frac{q_o S}{mV} C_{L_\delta}$, per sec
r_X	$\frac{I_{XZ}}{I_X}$
r_Z	$\frac{I_{XZ}}{I_Z}$
K_1	$\frac{g}{V}\cos\gamma$, per sec
K_2	$\frac{g}{V}\sin\gamma$, per sec
L_p'	$L_p+r_X N_p$, per sec
L_β'	$L_\beta+r_X N_\beta$, per sec^2
N_r'	$N_r+r_Z L_r$, per sec
N_β'	$N_\beta+r_Z L_\beta$, per sec^2
L_δ'	$L_\delta+r_X N_\delta$, per sec^2
N_δ'	$N_\delta+r_Z L_\delta$, per sec^2

TEST EQUIPMENT

The test airplane was a standard North American F–86A–5 airplane with external instrument booms added as shown in figure 1. The physical characteristics of this airplane are described in table I.

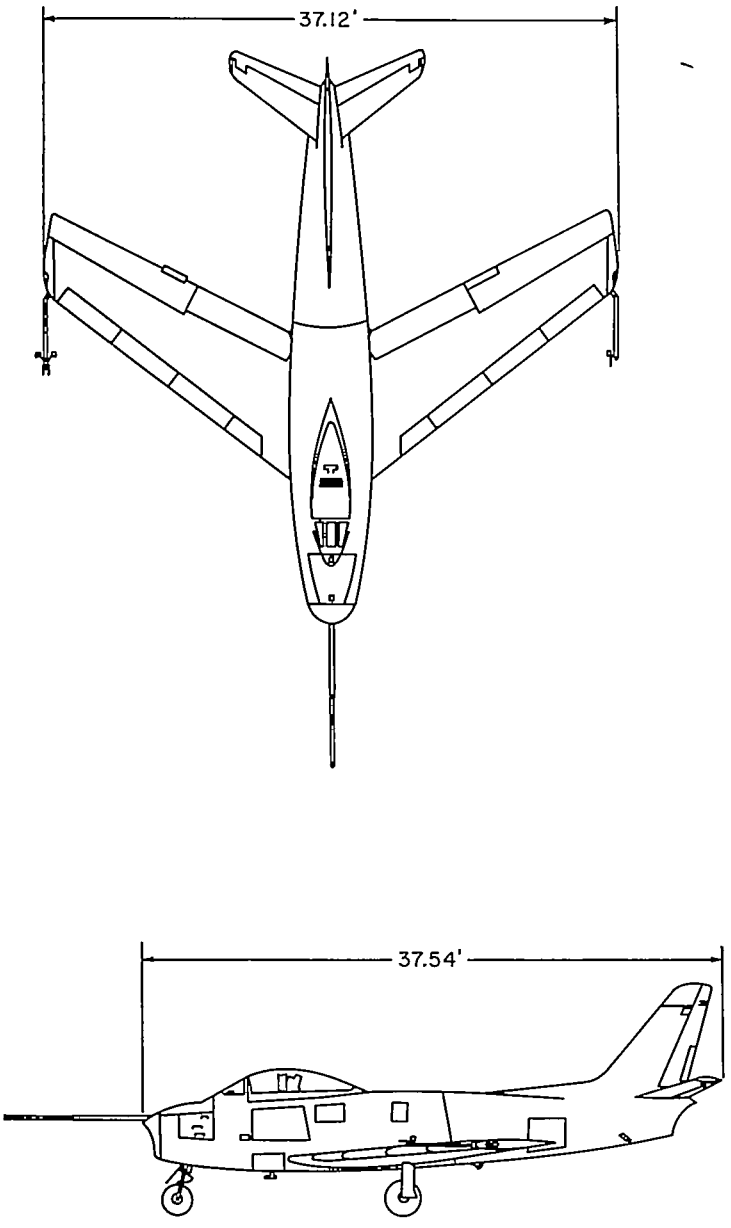

FIGURE 1.—Two-view drawing of test airplane.

Standard NACA instruments were used in measuring the following quantities: Pitching, rolling, and yawing velocities were measured by rate gyros with direct optical recording. Normal acceleration was measured by an air-damped vane-type accelerometer. Elevator, rudder, and aileron deflections were measured by control position transmitters that were linked directly to the control surfaces, and were recorded on an oscillograph. Angles of attack and sideslip were measured by a vane-type pickup and recorded on an oscillograph. True Mach number and altitude were obtained from the nose-boom airspeed system described in reference 1. All recordings were synchronized at 0.1-second intervals by a common timing circuit.

The rate gyros used to measure angular velocities and the accelerometer each had a sufficiently high natural frequency so that corrections to the data for instrument dynamics were not required. Tests of the control position recorders also indicated negligible dynamic lag through the frequency range of interest.

TEST PROCEDURES

The flight-test procedures consisted of recording airplane responses to pulse-type disturbances of each of the three control surfaces separately. Flights were made at an altitude of 35,000 feet through the Mach number range of 0.50 to 1.04. The trim lift coefficient varied from 0.51 to 0.12. A limited amount of data were also obtained at an altitude of 10,000 feet over this range.

During each test run one control surface was deflected and then returned to the trim position to provide a pulse input while the other two surfaces were held fixed. After application of the pulse, all three surfaces were held fixed until the oscillatory motion of the aircraft had essentially subsided. Sample time histories of airplane responses to the three control-surface inputs are shown in figures 2 and 3. The variation with Mach number of trim angle of attack and trim elevator angle are plotted in figure 4.

All flight runs at speeds below a Mach number of 0.95 were initiated from trimmed level flight, but to obtain data at the higher speeds it was necessary to dive the airplane. Altitude changes up to 2,000 feet were encountered during each diving run although there was little variation in Mach number. For analysis purposes the altitude and dynamic pressure were assumed constant at their average values during each run.

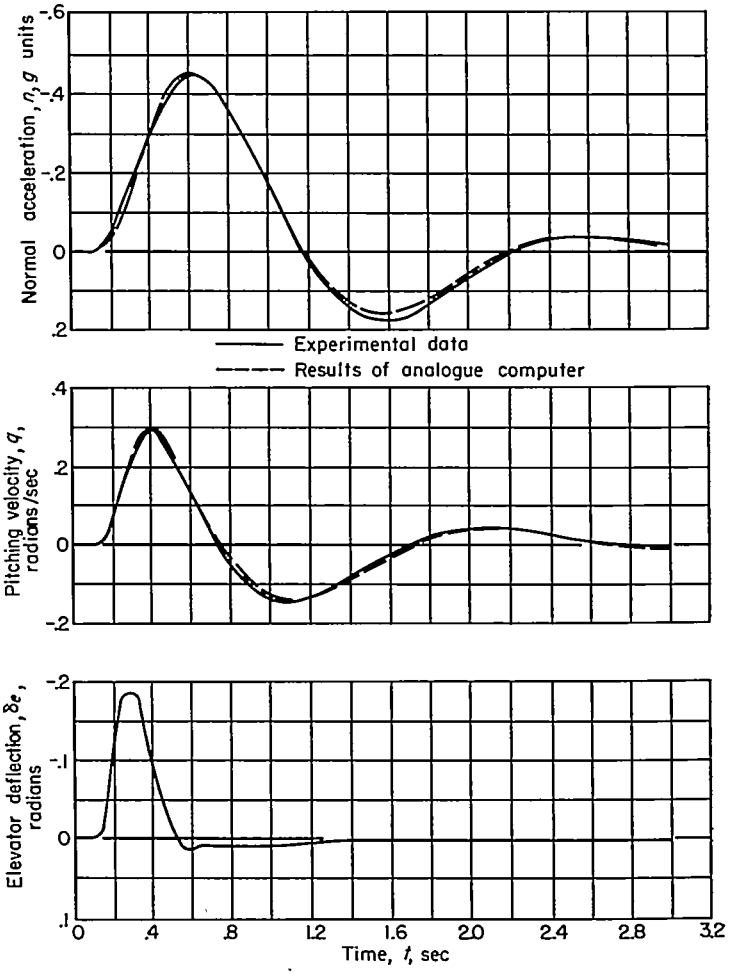

FIGURE 2.—Sample flight records of normal acceleration, pitching velocity, and elevator angle at a Mach number of 0.81.

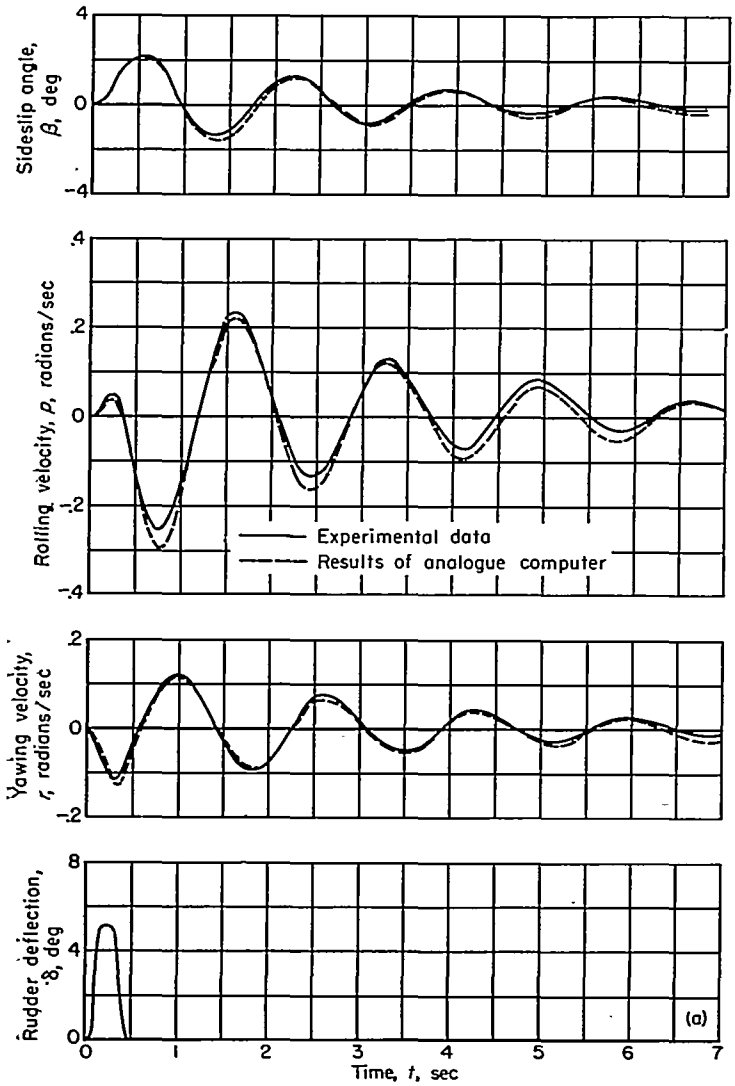

(a) Rudder input.

FIGURE 3.—Sample flight records of yawing velocity, rolling velocity, and sideslip angle at a Mach number of 0.81.

METHOD OF ANALYSIS

The procedures used in determining the airplane response characteristics from the measured transient time histories can be divided into three distinct steps which are outlined in the following sections. These are: frequency response calculations, evaluation of transfer functions, and a final check utilizing an analog computer. Wherever possible, stability derivatives are extracted from the coefficients of the transfer functions.

FREQUENCY RESPONSE CALCULATIONS

The first step involves the conversion of transient time histories into the frequency domain.

Under certain conditions a time function such as the pitching velocity $q(t)$ can be transformed into a complex frequency function $q(i\omega)$ by means of the Fourier integral relation

$$q(i\omega)=\int_0^\infty q(t)e^{-i\omega t}dt \qquad (1)$$

This integral must be evaluated from time zero to infinity for each frequency ω at which $q(i\omega)$ is desired. Obviously, the integration can be accomplished only if the behavior of $q(t)$ is known for an infinite time. Since $q(t)$ can be measured only for a finite time T, it is necessary for the system to reach steady-state conditions before time T such that $q(t)$ may be expressed analytically between the time limits T and infinity. In addition, the product $q(t)e^{-i\omega t}$ must converge as t approaches infinity.

Examination of the data used in this analysis showed that in every case the responses and the forcing function became constant after a finite time interval T. In the case of the pitching-velocity response to an elevator input these steady-state values may be expressed as $q(T)$ and $\delta_e(T)$, respectively, and thus equation (1) may be divided into two parts as follows:

$$q(i\omega)=\int_0^T q(t)e^{-i\omega t}dt+q(T)\int_T^\infty e^{-i\omega t}dt$$

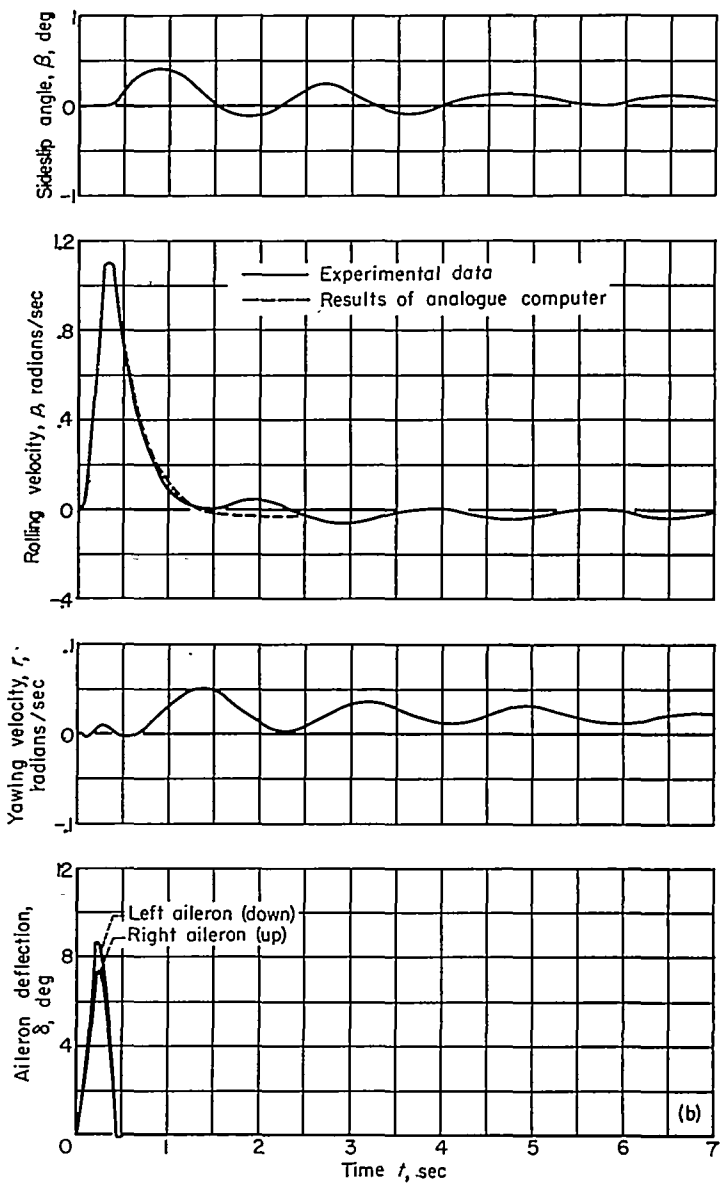

(b) Aileron input.

FIGURE 3.—Concluded.

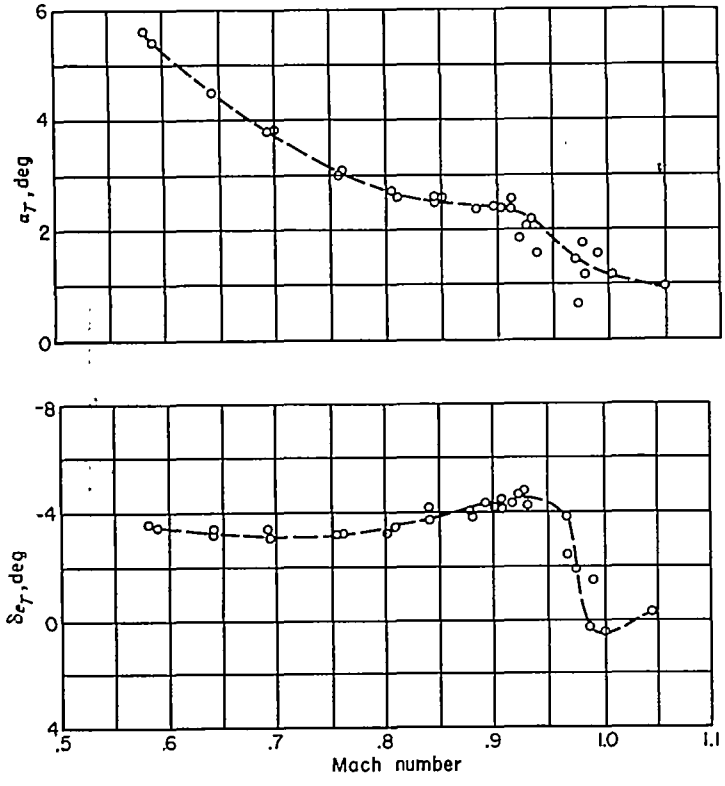

FIGURE 4.—Variation of trim angle-of-attack and trim elevator angle with Mach number.

The second integral can be evaluated analytically so that

$$q(i\omega)=\frac{q(T)}{i\omega}e^{-i\omega T}+\int_0^T q(t)e^{-i\omega t}dt \qquad (2)$$

For computational purposes equation (2) may be divided into its real and imaginary parts represented by the symbols R and I, respectively, so that

$$q(i\omega)=R+iI$$

where

$$R=-\frac{q(T)}{\omega}\sin\omega T+\int_0^T q(t)\cos\omega t\,dt$$

$$I=-\frac{q(T)}{\omega}\cos\omega T-\int_0^T q(t)\sin\omega t\,dt$$

The two integrals involving the transient part of $q(t)$ may may be evaluated by any of several approximation methods. In analyzing the data of this report, Simpson's rule was used to find the area under the product curves $q(t)\cos\omega t$ and $q(t)\sin\omega t$. Values of $q(t)$ were tabulated at 0.05-second intervals and the integrations were carried out at each integral value of frequency from 1 to 10 radians per second.

After obtaining the numerical values of R and I at each frequency, $q(i\omega)$ can be expressed in polar notation such that—

$$q(i\omega)=|q|e^{i\Phi_q}$$

where the amplitude, $|q|=\sqrt{(R)^2+(I)^2}$ and the angle, $\Phi_q=$ arc tan I/R.

The above integration process was repeated for the elevator forcing function $\delta_e(t)$ to determine

$$\delta_e(i\omega)=|\delta_e|e^{i\Phi_{\delta_e}}$$

The ratio of q/δ_e is then expressed as

$$\frac{q}{\delta_e}(i\omega)=\frac{q(i\omega)}{\delta_e(i\omega)}=\left|\frac{q}{\delta_e}\right|e^{i(\Phi_q-\Phi_{\delta_e})}=\left|\frac{q}{\delta_e}\right|e^{i\Phi_{q/\delta_e}}$$

where $|q/\delta_e|$ is the amplitude ratio and Φ_{q/δ_e} is the phase difference between the two quantities, $\Phi_q-\Phi_{\delta_e}$.

Similar calculations were made for the normal acceleration response to an elevator input and for the rolling, yawing, and sideslip responses to both rudder and aileron inputs.

In order that flight-test results can be correlated directly with wind-tunnel measurements it is sometimes desirable to correct the angular velocities measured in flight so that they conform to the system of stability axes rather than the body axes about which the recording instruments are alined. The necessary correction is described in Appendix A.

A further consideration in frequency-response calculations is the shape of the forcing function. As discussed in Appendix B, the type of input used in flight definitely places a limit on the accuracy of the Fourier analysis. In general, to obtain the widest usable frequency range, a pulse input should be used. When low frequencies are desired, a step input is preferable, although this type of disturbance may result in motions that exceed the ranges of linearity.

The final result of the above calculations is a graphical representation of the airplane transfer function (frequency response) for a given test condition. This is plotted as curves of amplitude ratio and phase angle versus frequency. The remainder of this section of the report is concerned with the determination of analytical expressions for these curves.

Reference 2 is one of many sources that explain in more detail the use of the Fourier transform for problems of this type.

DETERMINATION OF TRANSFER-FUNCTION COEFFICIENTS

Dynamic-response templates.—A graphical method was used to find the type of transfer function that best defines each of the measured frequency responses. Numerical values of the transfer coefficients were also determined in the same operation. This method involved the use of a set of templates developed by C. S. Draper of the Instrumentation Laboratory of the Massachusetts Institute of Technology. These templates are described fully in reference 3, and their design is based on the following considerations:

1. A rational function of complex frequency D can, in general, be expressed as

$$F(D)=K\frac{(D+a_1)(D+a_2)\ldots(D+a_n)}{(D+b_1)(D+b_2)\ldots(D+b_m)} \qquad (3)$$

where the a_i and b_i may be either real or complex, and, if complex, always appear as conjugate pairs and where K is any real number. When a_i is a real number, a factor $(D+a_i)$ may be expressed as

$$\frac{1}{\tau}(1+\tau D)$$

where $\tau=\frac{1}{a_i}$. When a_i and a_{i+1} are a complex conjugate pair the two factors $(D+a_i)(D+a_{i+1})$ can be expanded, by introducing new coefficients, into the form $(D^2+2\zeta\omega_n D+\omega_n^2)$

where $\omega_n^2=a_ia_{i+1}$ and $2\zeta\omega_n=a_i+a_{i+1}$. Factoring out ω_n^2 then gives

$$\omega_n^2\left(1+2\zeta\frac{D}{\omega_n}+\frac{D^2}{\omega_n^2}\right)$$

The terms $\frac{1}{\tau}$ and ω_n^2 that appear outside the parentheses, being real numbers, may be grouped together with the multiplying factor K. When an a_i or b_i is zero then a factor D will be present in either the numerator or the denominator. Then, $F(D)$ in factored form will consist entirely of combinations of the three forms.

Since we are interested only in the steady-state frequency response, the complex variable D can be replaced by the frequency variable $i\omega$, (where $i=\sqrt{-1}$) and each of the three factors may be written in polar form as follows:

For $(1+\tau D)$,

$$1+\tau i\omega=\sqrt{1+\tau^2\omega^2}\,e^{i\Phi_1} \tag{4}$$

where

$$\Phi_1=\tan^{-1}\tau\omega$$

for $\left(1+2\zeta\frac{D}{\omega_n}+\frac{D^2}{\omega_n^2}\right)$,

$$1+2\zeta\frac{i\omega}{\omega_n}+\left(\frac{i\omega}{\omega_n}\right)^2=\sqrt{\left(1-\frac{\omega^2}{\omega_n^2}\right)^2+4\zeta^2\frac{\omega^2}{\omega_n^2}}\,e^{i\Phi_2} \tag{5}$$

where

$$\Phi_2=\tan^{-1}\frac{2\zeta(\omega/\omega_n)}{1-(\omega^2/\omega_n^2)}$$

and for D

$$i\omega=\omega e^{i\Phi_3} \tag{6}$$

where

$$\Phi_3=\tan^{-1}\infty=90°$$

2. When $\tau\omega$ is taken as a nondimensional frequency variable, all first-order terms of the form $(1+\tau i\omega)$ can be defined by a single amplitude curve and a single phase-angle curve as shown in figure 5. In a similar manner all possible second-order terms of the form $1+2\zeta\frac{i\omega}{\omega_n}+\left(\frac{i\omega}{\omega_n}\right)^2$ can be defined by a family of curves with ω/ω_n as the nondimensional frequency variable. There will be a different pair of curves for each value of damping ratio ζ, as shown in figure 6. For the factor $i\omega$ (eq. (6)) the amplitude is simply equal to ω and the phase angle is a constant 90°.

3. Since a typical transfer function may consist of more than one of these factors in both numerator and denominator, it is of great advantage to plot the amplitudes to a logarithmic scale so that multiplication or division of factors of the type shown in equations (4) to (6) may be accomplished by mere graphical addition of the amplitudes. The nondimensional frequency has also been plotted to a logarithmic scale as shown in figures 5 and 6. Then as frequency approaches either zero or infinity the amplitudes become asymptotic to straight lines. In both figures as frequency decreases the amplitudes approach asymptotically the value of unity. At high frequencies the amplitude of $(1+\tau i\omega)$ is essentially equal to $\tau\omega$ and thus it plots as a striaght line of slope 1 (fig. 5). Similarly, the amplitude of a second-order term approaches the value $\left(\frac{\omega}{\omega_n}\right)^2$ as frequency increases and is asymptotic to a straight line of slope 2. Since a second-order term of this type normally appears in the denominator, it has been plotted as

$$\left[1+2\zeta\frac{i\omega}{\omega_n}+\left(\frac{i\omega}{\omega_n}\right)^2\right]^{-1}$$

and thus the slope of the amplitude curve is −2 (fig. 6). In both plots the asymptotes intersect at unity on the nondimensional frequency scale. This intersection is termed "the breakpoint."

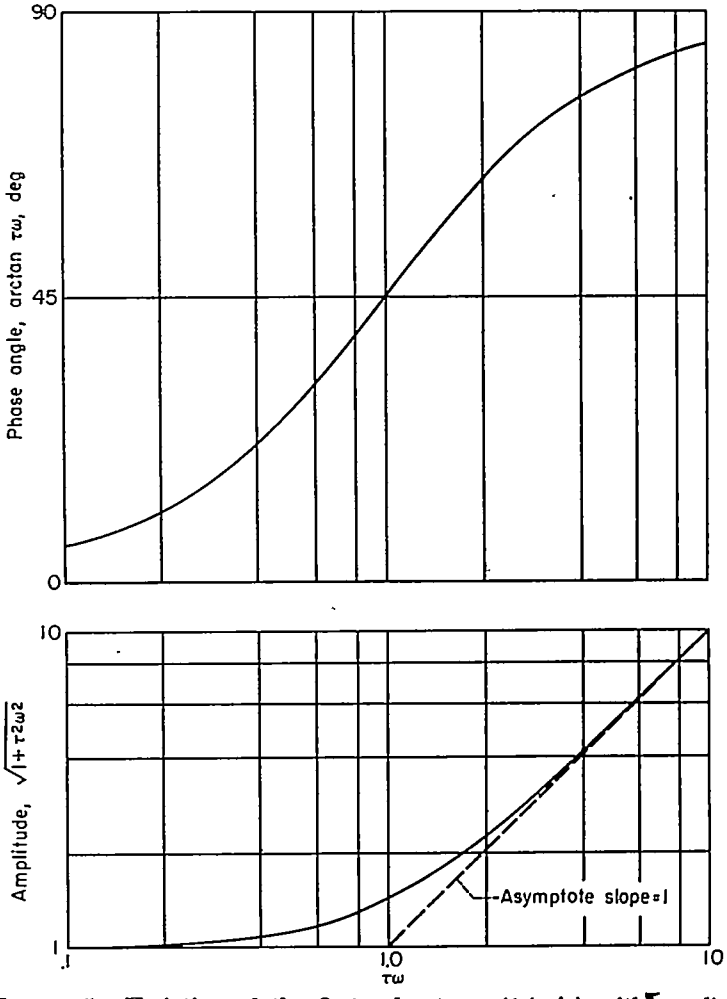

FIGURE 5.—Variation of the first-order term $(1+\tau i\omega)$ with nondimensional frequency $\tau\omega$.

The phase angles are plotted to a linear scale because when factors of the types shown in equations (4) to (6) are combined, the resultant phase angle of $F(D)$ is merely the algebraic sum of the individual angles. It can be seen in figures 5 and 6 that the angles of these first- and second-order terms approach 90° and −180°, respectively, at high frequencies. Thus an amplitude slope of 1 corresponds to an angle of 90°, while a slope of −2 corresponds to an angle of −180°. In general, as ω approaches infinity the amplitude of $F(D)$ approaches $K\omega^{(n-m)}$, where n and m are defined in equation (3). Then the amplitude slope is equal to $(n-m)$ on the logarithmic plot and the phase angle is $90(n-m)°$.

The templates used in the analysis of the data were accurate representations of the curves shown in figures 5 and 6 cut from transparent material with the breakpoints marked. Twelve pairs of second-order templates were included in the set to give values of damping ratio from 0.1 to 1.0 in increments of 0.1 and in addition values of 0.05 and 0.15.

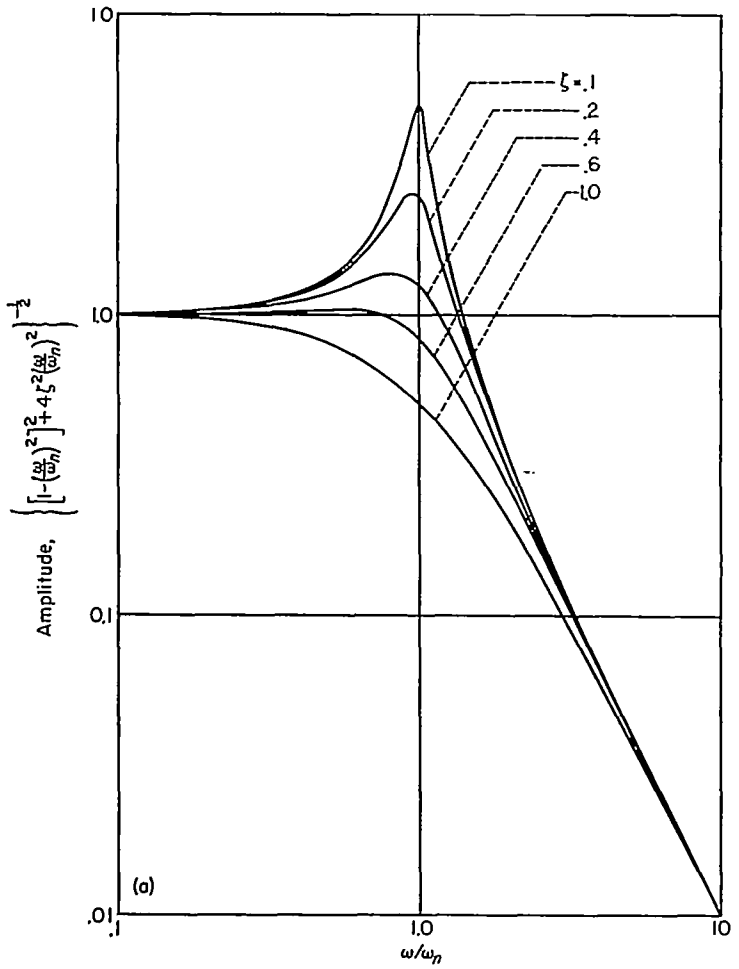

(a) Amplitude.

FIGURE 6.—Variation of the second-order term $\left[1+2\zeta\frac{i\omega}{\omega_n}+\left(\frac{i\omega}{\omega_n}\right)^2\right]^{-1}$ with nondimensional frequency for various values of damping ratio.

The computed frequency-response data (amplitude ratios and phase angles) were plotted to the same logarithmic scale as the templates, and then by a trial-and-error approach the template or combination of templates that best matched the given data was determined. To determine the proper combination, various amplitude templates were positioned in such a way that their algebraic sum matched the experimental amplitude ratio curve. For each amplitude template the corresponding phase-angle template was placed on the experimental phase-angle curve so that the breakpoint of each pair was alined with respect to frequency. The various pairs of templates were then adjusted until the sum of the individual amplitudes and phase angles most nearly matched the test data. The frequency at which the breakpoint of each pair occurred (ω_B) was noted and then the appropriate values of τ and ω_n were determined directly, since for each first-order term

$$\tau=\frac{1}{\omega_B}$$

and for each second-order term

$$\omega_n=\omega_B$$

In general, each factor will have a different breakpoint.

At first glance, this procedure may seem extremely tedious but it has been found that with practice one can determine coefficients quite rapidly in this manner. For a more complete description of the principles involved in this type of graphical representation reference 4 is recommended.

Analog Computer.—As a final step in the calculations a Reeves analog computer was used to refine the previously determined values of transfer-function coefficients. This was accomplished by placing the actual time histories of the control motion into the computer by means of an input table. Then this input was fed into a circuit representing the equations of motion as obtained in the previous step and the outputs of the machine were obtained. These outputs were compared to the actual time histories of the airplane responses as obtained in flight. By changing dial settings on the computer the transfer coefficients could be adjusted until the output of the computer most nearly matched the actual flight data. (Such a comparison is shown in figs. 2 and 3.) Thus, in addition to providing a refinement of the coefficients obtained with the templates, this step also resulted in a check of all previous calculations. In general, operations of this type can be conveniently accomplished on the computer only when the form of the transfer function is known.

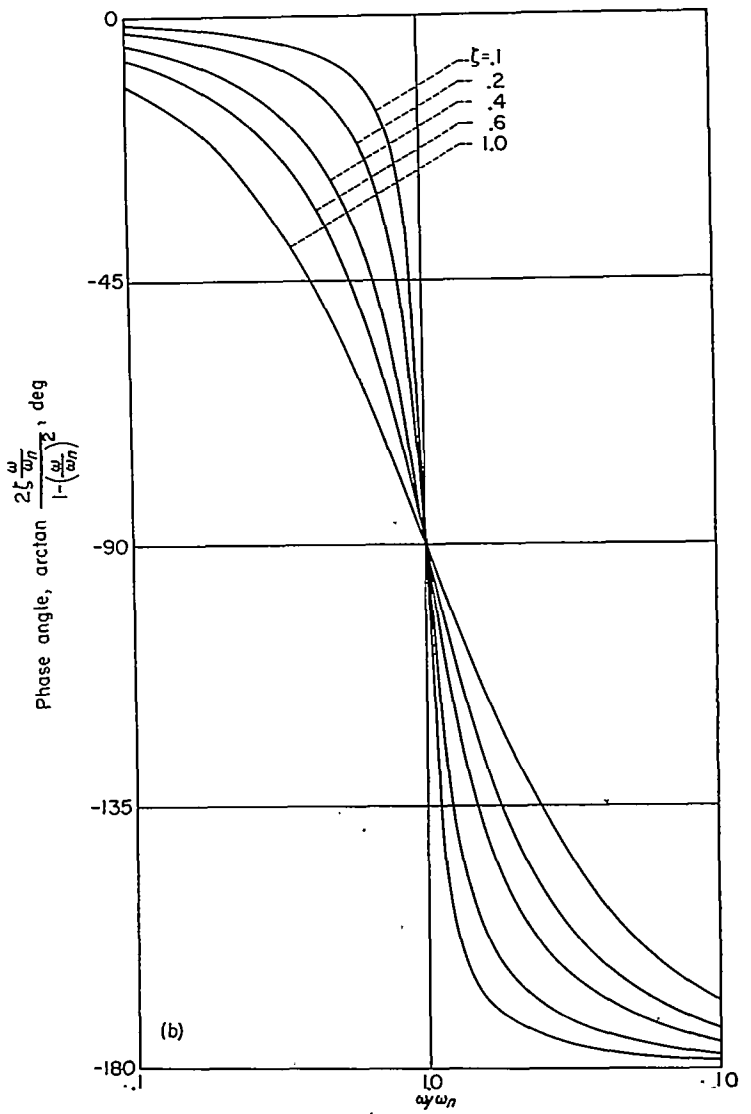

(b) Phase angle.

FIGURE 6.—Concluded.

RESULTS AND DISCUSSION

In the following paragraphs the longitudinal characteristics and the lateral-directional characteristics are discussed separately. Flight-evaluated frequency responses, transfer functions, and stability derivatives are presented and compared with predictions based on wind-tunnel data and theoretical studies.

LONGITUDINAL RESPONSE CHARACTERISTICS

Frequency response.—Plotted in figure 7 are typical flight-evaluated frequency responses of pitching velocity and normal acceleration to elevator inputs. The purpose of these figures is to show general trends with varying Mach number, and therefore smooth curves have been faired through the calculated test points. In most cases more than one flight record was analyzed at each flight speed and only at the highest speeds was there appreciable inconsistency. Each transient record was analyzed through the frequency range of 1 to 10 radians per second and some scatter in the data was noted at either end of the frequency range. For this reason, as well as for clarity, portions of some of the responses have been omitted from figure 7.

The amplitude-ratio plots show the increase in natural frequency and the decrease in amplitude which reflect the changes in static margin and elevator effectiveness with Mach number.

To afford a comparison with estimates made from wind-tunnel data, typical frequency responses for a Mach number of 0.81 have been replotted in figure 8. Shown here are the actual data points obtained from a single transient input. Also shown as solid lines are responses predicted by use of the stability derivatives of table II (ref. 5) and transfer functions developed in Appendix C. The scatter between individual data points is typical for responses in the lower speed range; at Mach numbers near 1.0, however, there was somewhat more scatter in the individual data points.

Transfer functions and stability derivatives.—The airplane transfer functions were determined from the frequency responses of figure 7 by using the templates described in the Analysis Section. Final values of the coefficients were obtained from the analog computer by matching the original time histories. It was found that the airplane responses could be adequately defined by transfer functions of the form:

$$\frac{q}{\delta_e}=\frac{C_{1q}D+C_{oq}}{D^2+bD+k}$$

and

$$\frac{n}{\delta_e}=\frac{C_{on}}{D^2+bD+k}$$

As indicated in figure 2 the output of the analog computer closely matched the transient motions measured in flight. These equations are also of the same form as the theoretical transfer functions developed in Appendix C.

The variation with Mach number of the coefficients ω_n and ζ are plotted in figure 9. The damping-ratio curve was faired in accordance with additional data which more clearly defined the sharp variations between Mach number of 0.88 and 0.95. An indication of the consistency of the data is given by the scatter of the points at each flight speed.

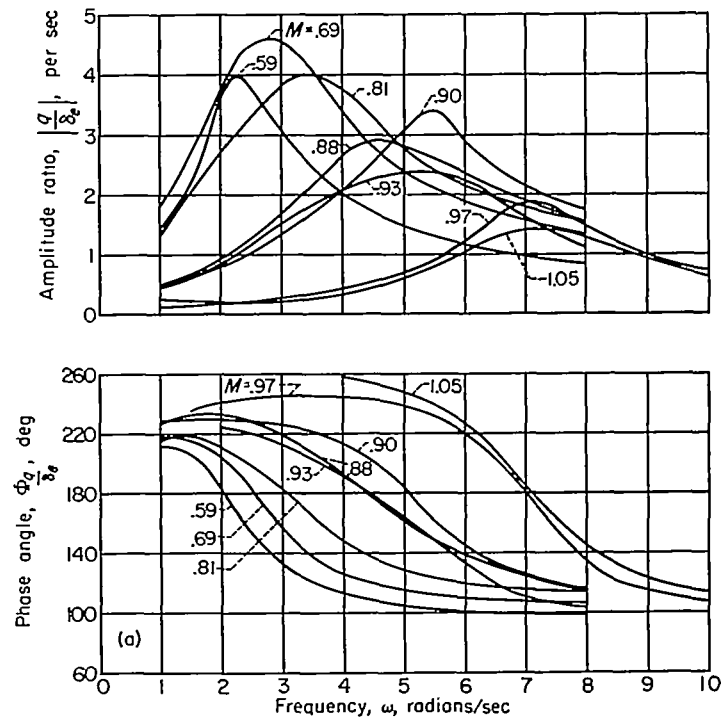

(a) Pitching velocity response to elevator input.

FIGURE 7.—Longitudinal frequency responses at various flight Mach numbers at an altitude of 35,000 feet.

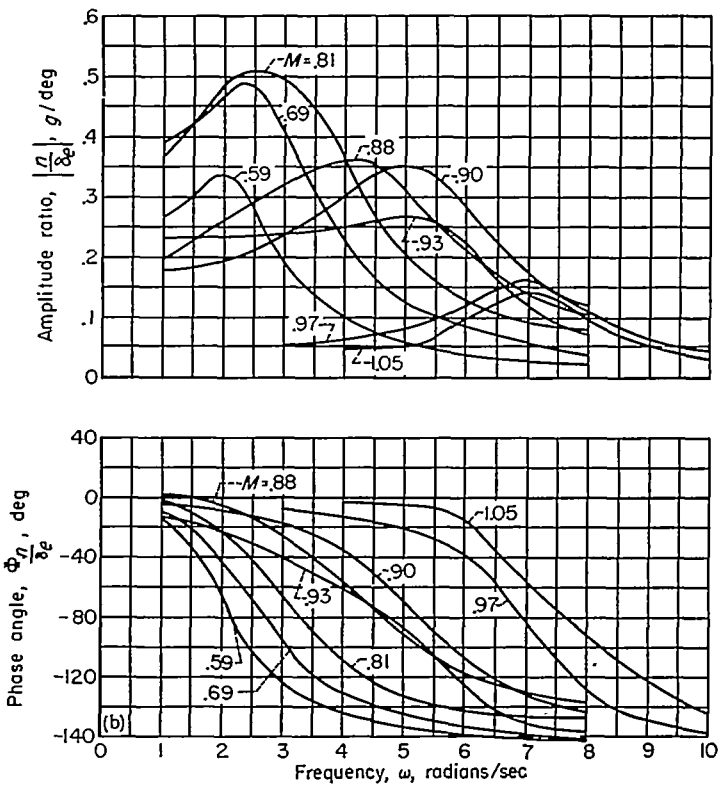

(b) Normal acceleration response to elevator input.

FIGURE 7.—Concluded.

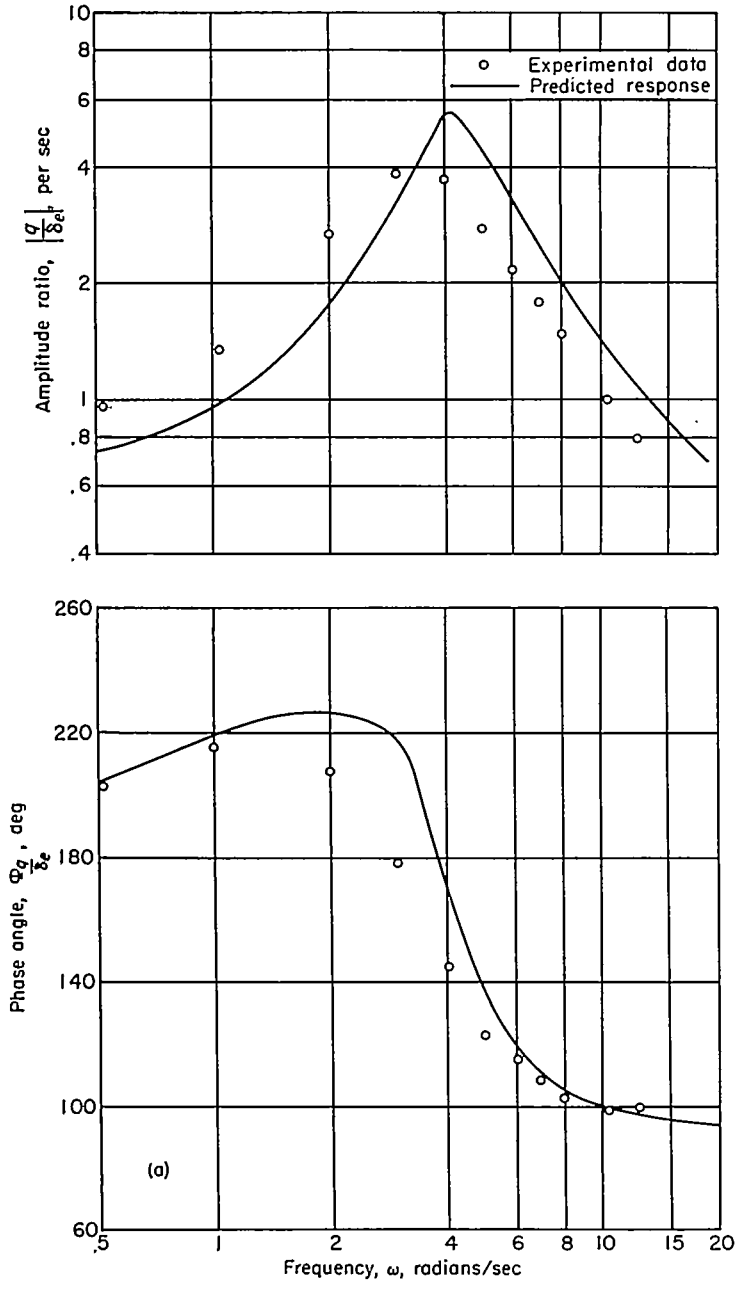

(a) Pitching velocity response.

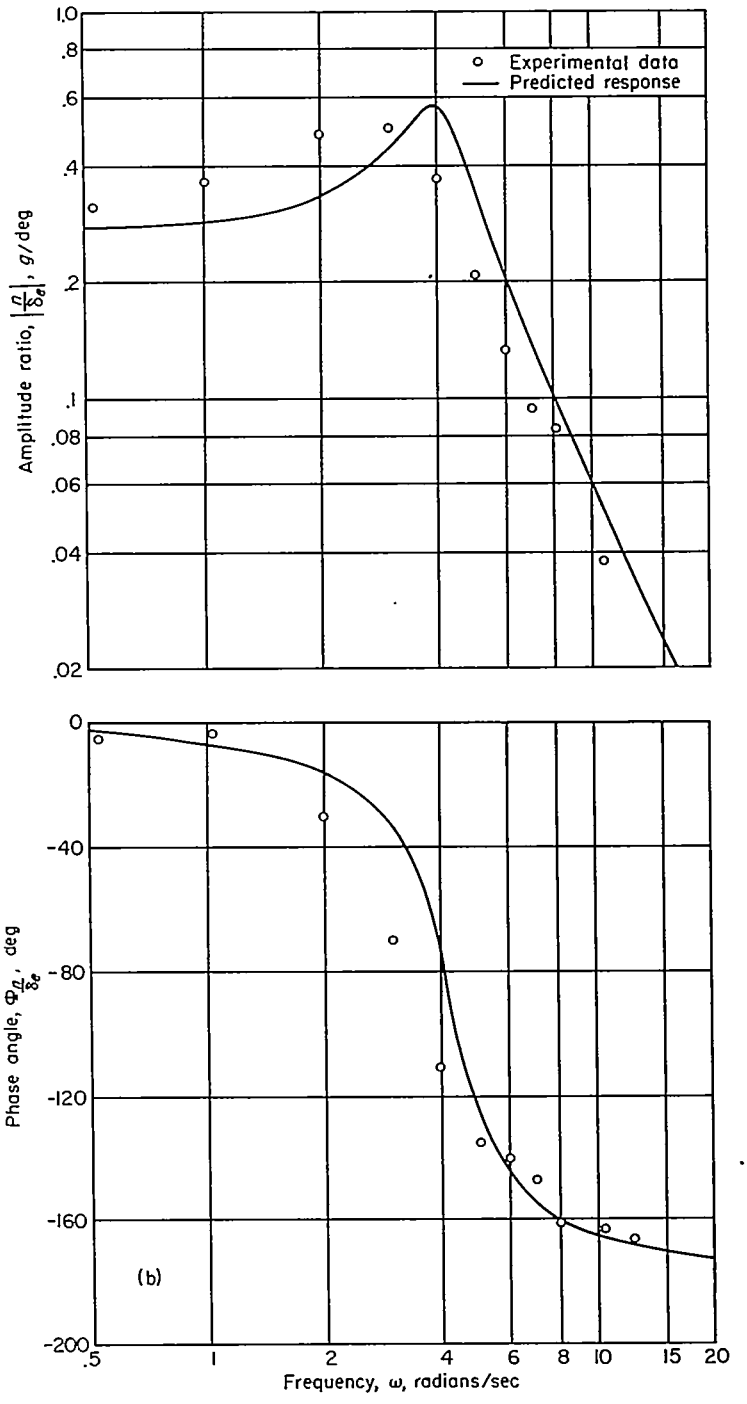

(b) Normal acceleration response.

FIGURE 8.—Comparison of experimental and predicted longitudinal frequency responses at a Mach number of 0.81 (altitude 35,000 feet).

FIGURE 8.—Concluded.

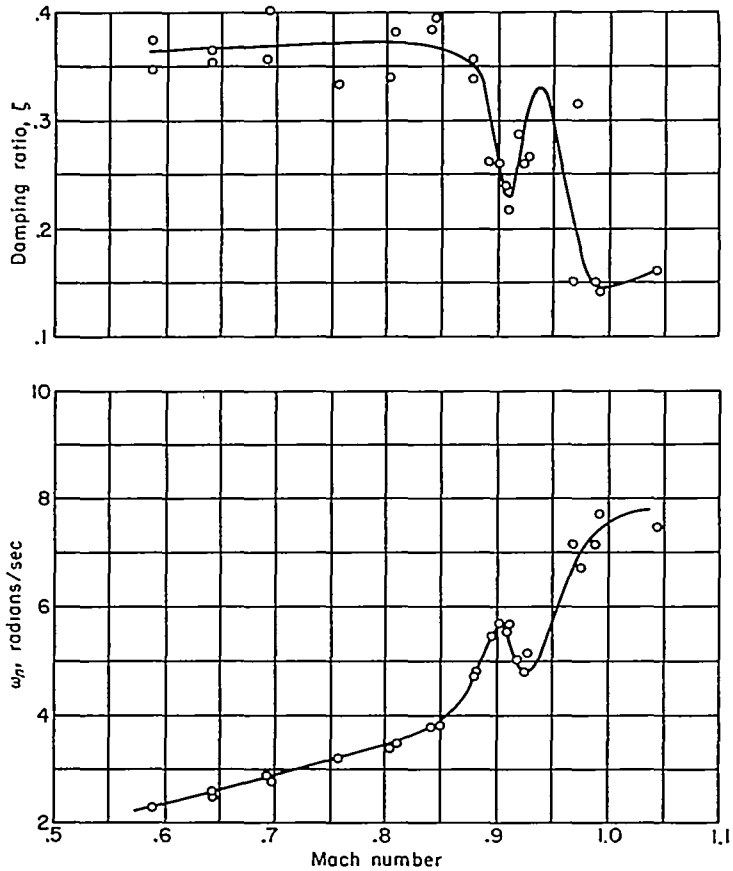

FIGURE 9.—Variation of longitudinal undamped natural frequency and damping ratio with Mach number.

Plotted in figures 10 and 11 are the stability derivatives C_{m_α}, $C_{m_{\delta_e}}$, and $C_{m_q}+C_{m_{\dot{\alpha}}}$. These were evaluated from the transfer coefficients as indicated in Appendix C. Because of the difficulty in finding reliable values of the coefficient C_{o_q}, wind-tunnel values of C_{L_α} (also shown in fig. 10) were used to calculate $C_{m_q}+C_{m_{\dot{\alpha}}}$. Comparisons are made with estimates shown in table II and in the case of C_{m_δ} the results of this investigation are compared to unpublished static flight data.

LATERAL DIRECTIONAL RESPONSE CHARACTERISTICS

Frequency responses.—Plotted in figure 12 are typical flight-evaluated frequency responses of rolling velocity, yawing velocity, and sideslip angle to rudder and also to aileron inputs. These were all obtained at an altitude of 35,000 feet; responses at 10,000 feet showed similar characteristics and have not been plotted. As in the case of the longitudinal frequency responses smooth curves have been faired through the calculated test points.

The responses to rudder inputs have not been plotted at frequencies greater than 8 radians per second because there was considerable scatter and also a lack of well-defined trends in the data at the higher frequencies. The aileron responses, however, are shown to 16 radians per second. Wherever necessary for clarity or because of erratic data, parts of some of the curves have been omitted. The β/δ_a response is shown at only three speeds because of a failure in the sideslip-angle recording system.

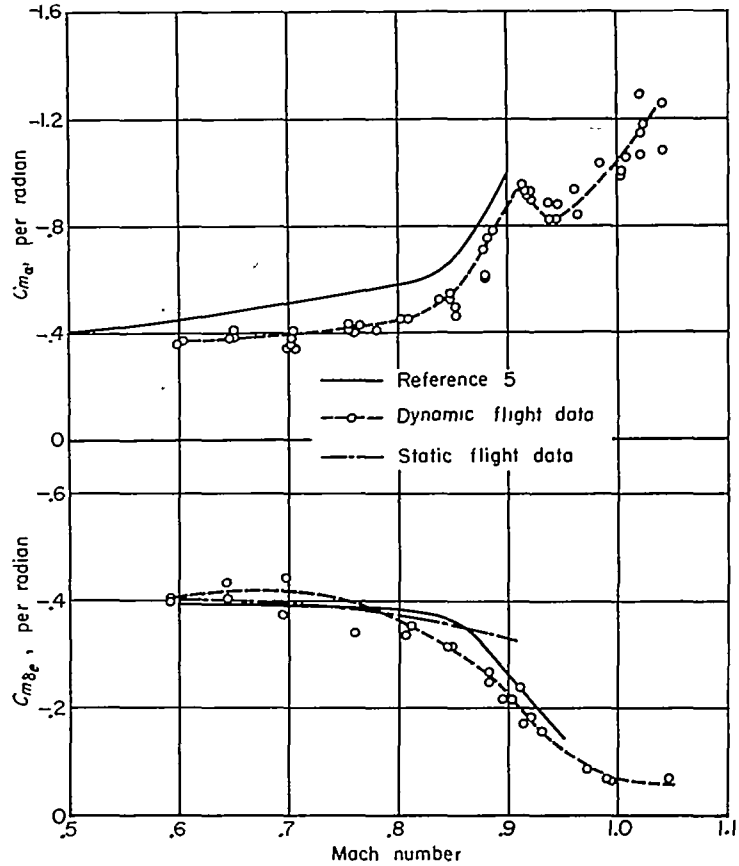

FIGURE 10.—Variation with Mach number of the stability derivatives C_{m_α} and $C_{m_{\delta_e}}$ h wit Mach number.

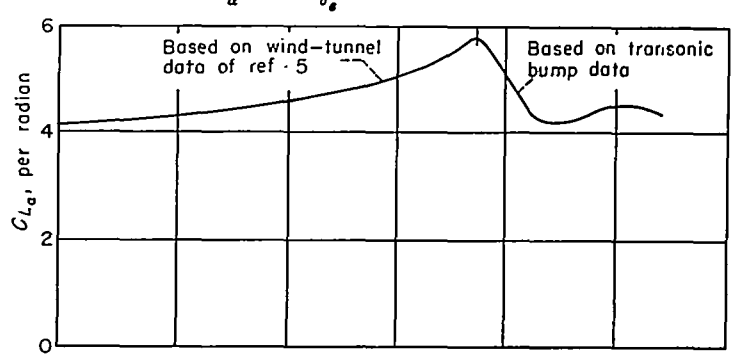

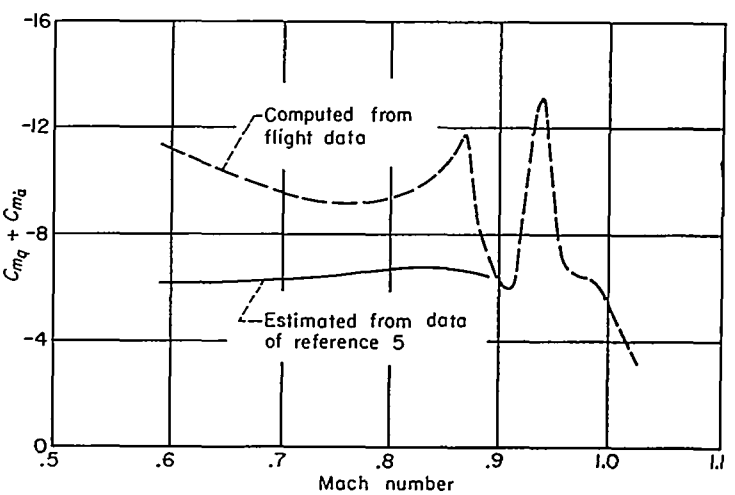

FIGURE 11.—Variation with Mach number of the stability derivatives C_{L_α} and $C_{m_q}+C_{m_{\dot{\alpha}}}$ with Mach number.

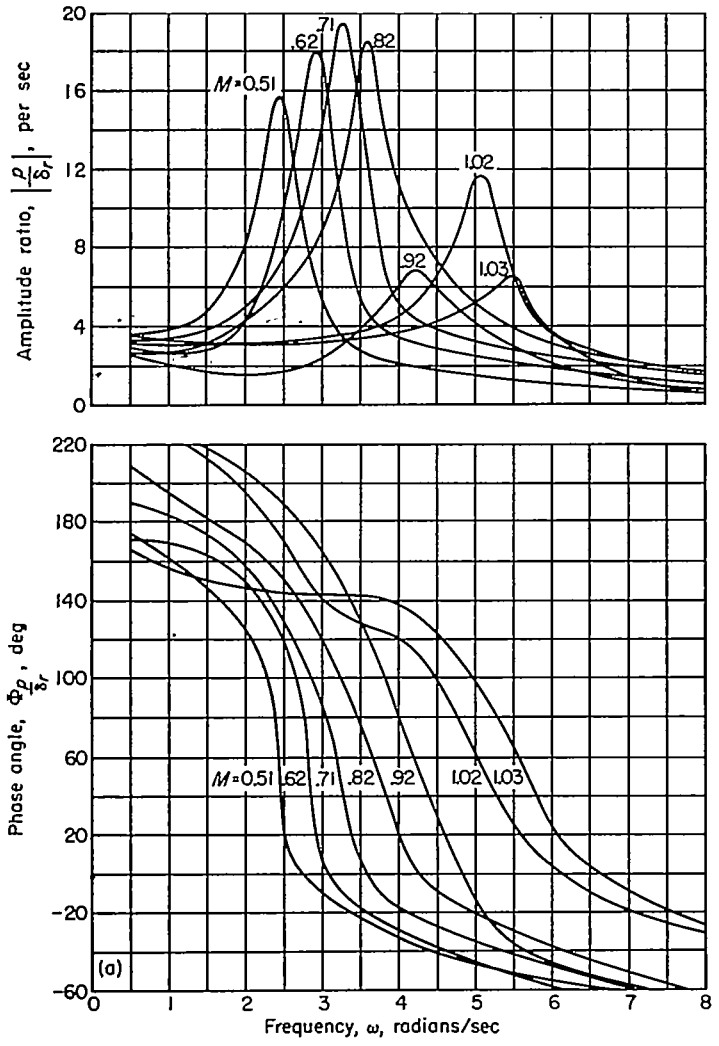

(a) Rolling velocity response to rudder input.

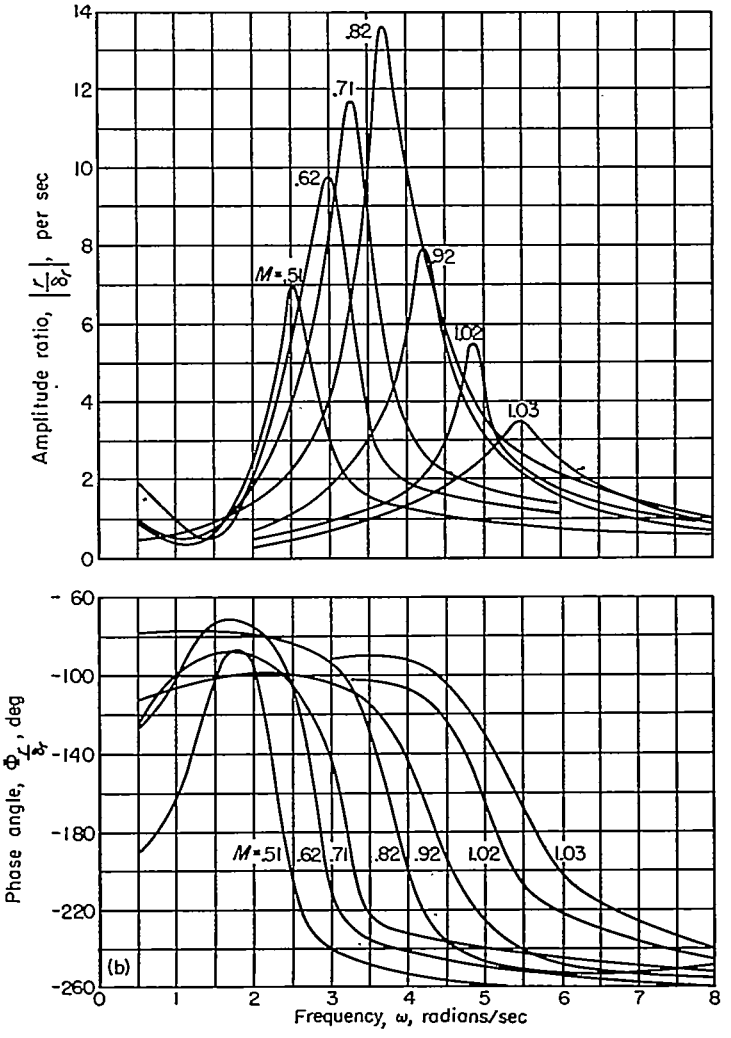

(b) Yawing velocity response to rudder input.

FIGURE 12.—Lateral-directional frequency responses at various flight Mach numbers (altitude 35,000 feet).

FIGURE 12.—Continued.

With minor exceptions, the curves show consistent and gradual variations with Mach number. One such exception can be seen in figures 12 (d) and 12 (e) where the amplitudes of p/δ_a and r/δ_a at a Mach number of 0.61 lack the customary resonant peaks. This is the result of time histories in which there was no oscillatory motion. This unusual characteristic can be explained by reference to the predicted transfer functions developed in Appendix C and discussed in the following section. The predicted p/δ_a response equation for a Mach number of 0.6 at 35,000 feet is

$$\frac{p}{\delta_a}=\frac{21.1D(D^2+0.455D+6.74)}{(D+0.00113)(D+2.203)(D^2+0.438D+7.25)}$$

It can be seen that the two quadratic terms are nearly identical and thus the oscillatory mode is effectively canceled. Since rolling and yawing motions are coupled, the r/δ_a response must exhibit the same characteristics at this particular speed.

Another interesting point with regard to figure 12 (e) is the wide variation in phase angles at different flight speeds. Predicted transfer functions indicate that at low speeds (below a Mach number of 0.7) where $C_{n_{\delta_a}}$ is negative, the phase angles approach −270° asymptotically with increasing frequency. Unpublished wind-tunnel data indicate that near a Mach number of 0.7 there is a transition in which $C_{n_{\delta_a}}$ becomes positive and consequently three of the coefficients in the numerator of the transfer function change sign. The result is an increase of 180° in the high-frequency phase lag.

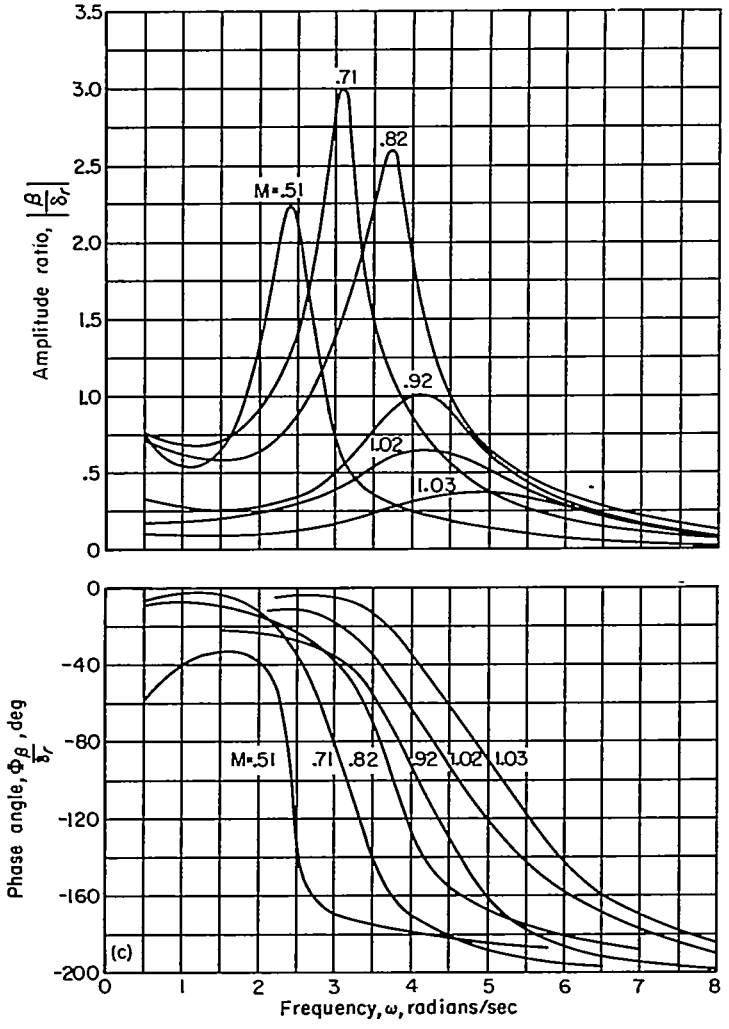

(c) Sideslip angle response to rudder input.

FIGURE 12.—Continued.

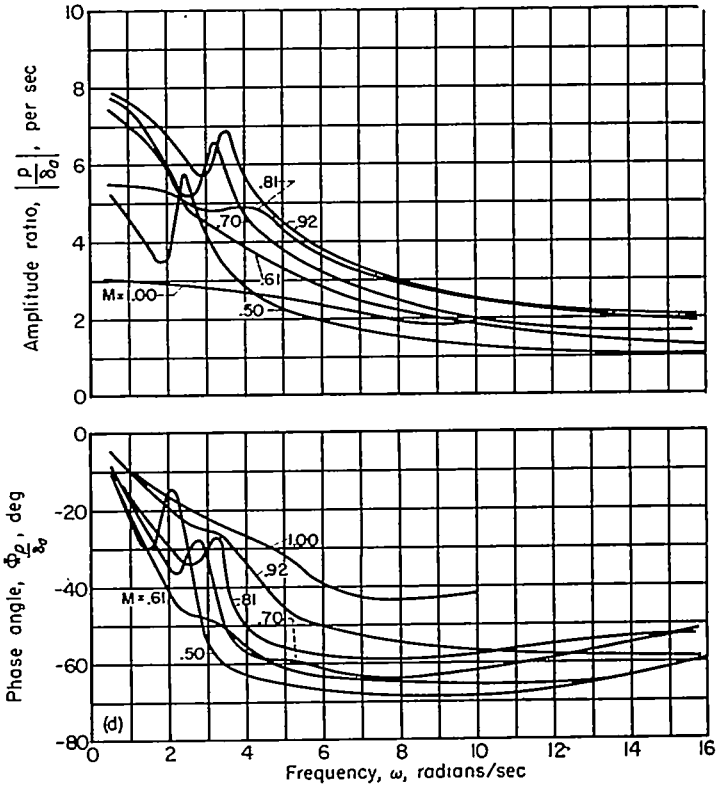

(d) Rolling velocity response to aileron input.

FIGURE 12.—Continued.

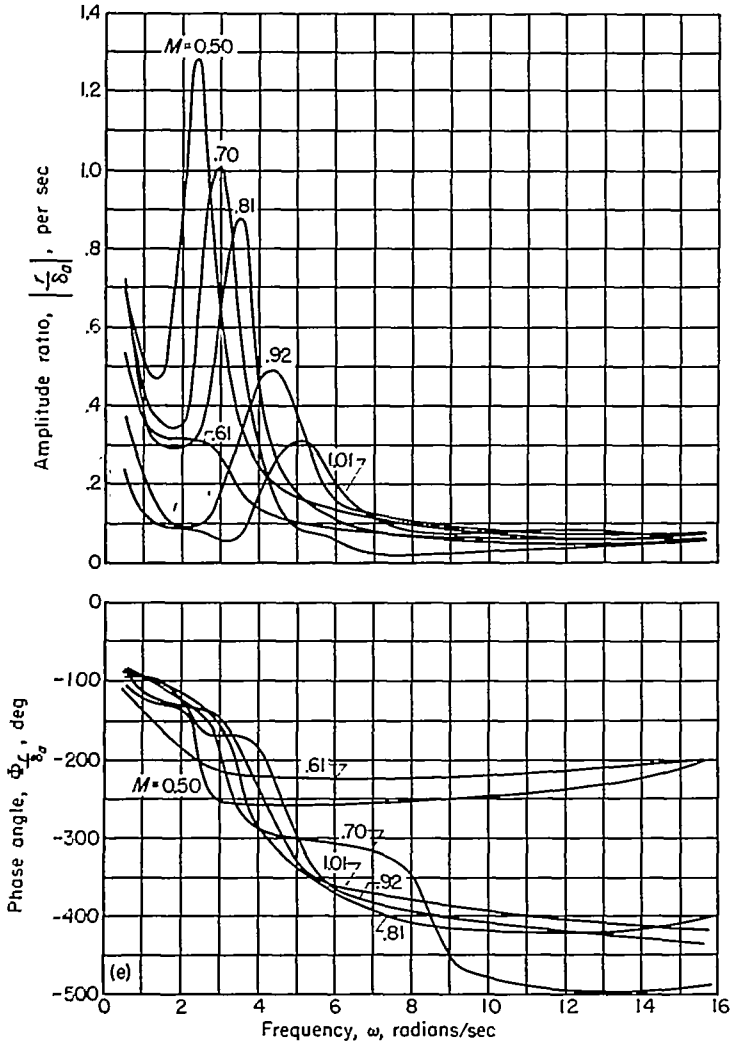

(e) Yawing velocity response to aileron input.

FIGURE 12.—Continued.

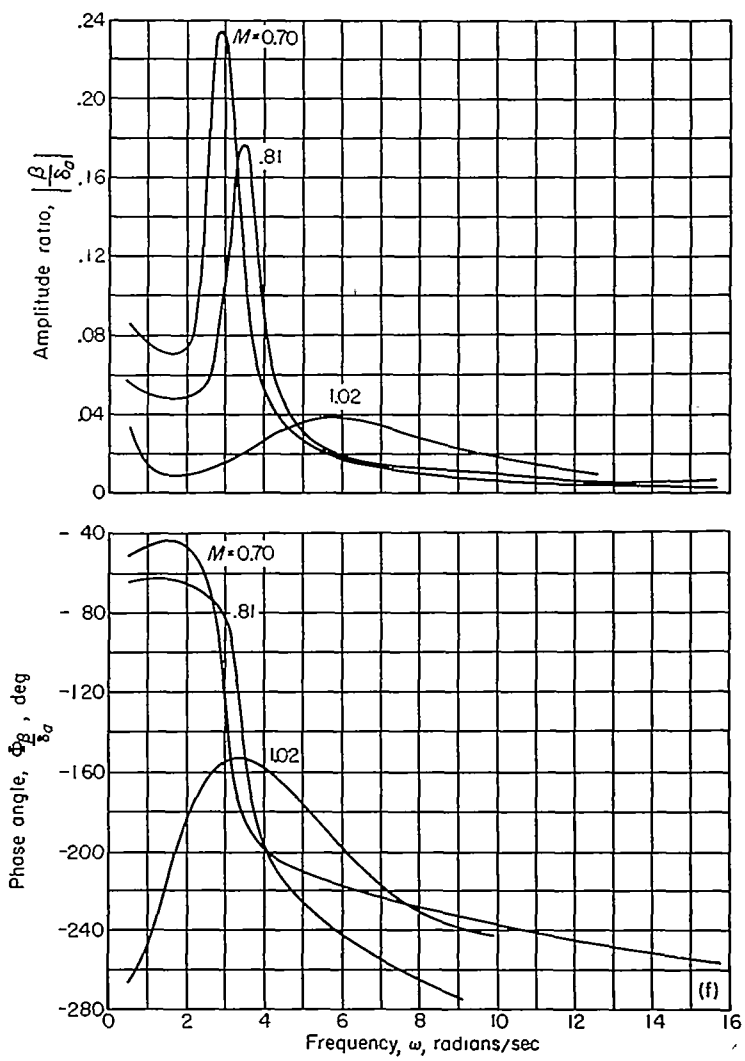

(f) Sideslip angle response to aileron input.

FIGURE 12.—Concluded.

The frequency-response test points derived from flight data at a Mach number of 0.81 have been replotted in figure 13 which shows all six responses for the 35,000-foot altitude. These results are typical in indicating the degree of scatter usually encountered in the Fourier analysis of a particular flight record. Plotted as solid lines for comparison are predicted responses that have been calculated using estimates of the various stability derivatives presented in table II, which were obtained from reference 6 and also from wind-tunnel tests by the manufacturer. These calculations were made as shown in Appendix C, using the exact linear fourth-order response equations. The agreement between measured and predicted responses is generally good except, in some cases, at the extremes of the test frequency range. This is particularly noticeable in figure 13 (d) where the measured frequency response of p/δ_a indicates a mode of motion not consistent with the rigid-body equations of Appendix C. The increase in phase angle and the "up-turn" in the amplitude curve at high frequencies indicate the presence of an additional mode which is probably related to the primary bending frequency of the wing (about 8 cps).

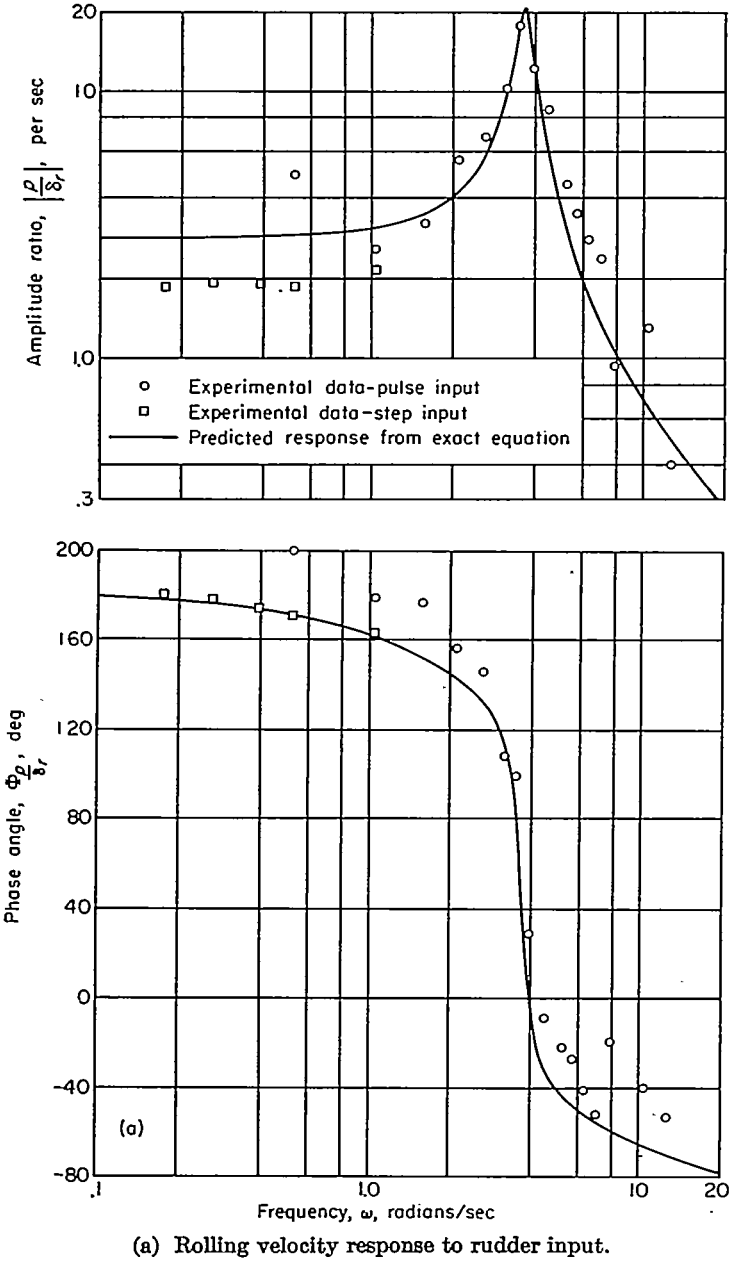

(a) Rolling velocity response to rudder input.

FIGURE 13.—Comparison of experimental and predicted lateral directional frequency responses at a Mach number of 0.81 (altitude 35,000 feet).

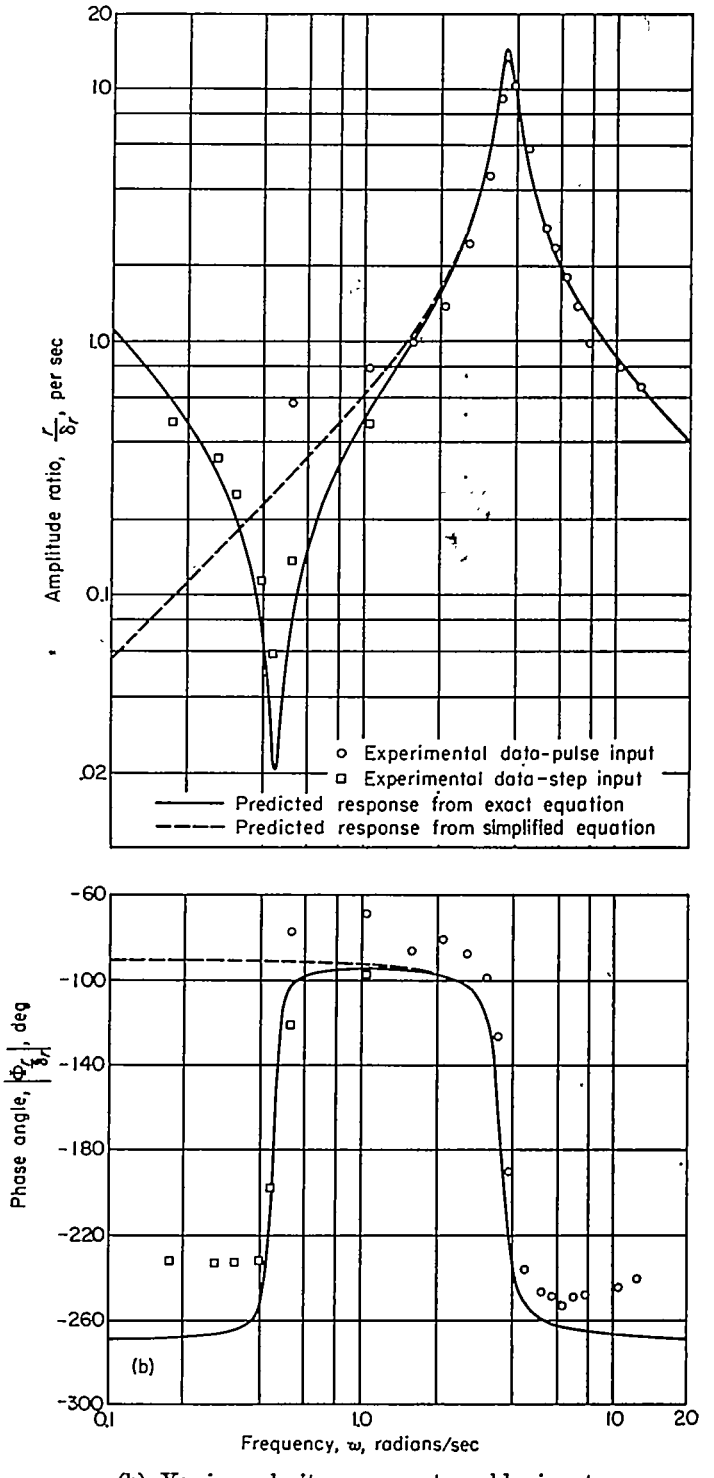

(b) Yawing velocity response to rudder input.

FIGURE 13.—Continued.

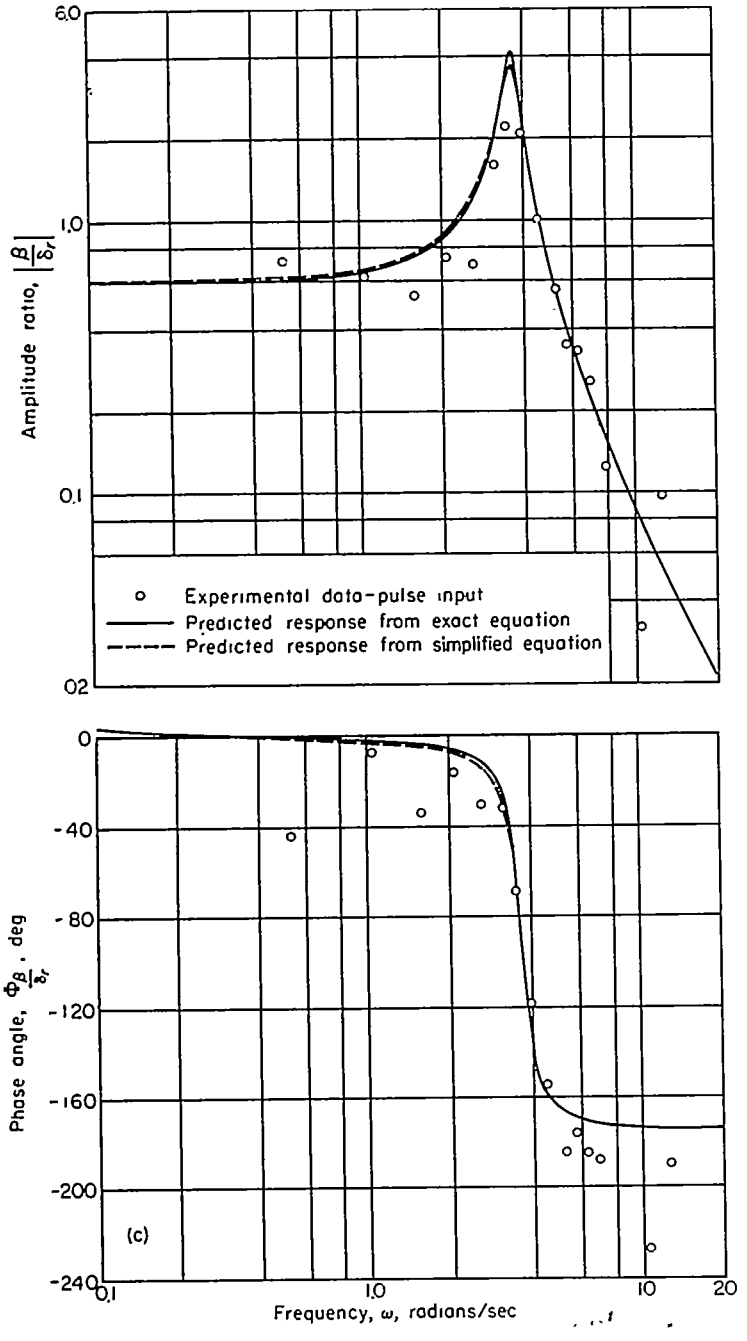

(c) Sideslip angle response to rudder input.

FIGURE 13.—Continued.

In addition to the pulse-type inputs, a step disturbance of the rudder was used in one instance at a Mach number of 0.81 in order to define more clearly the low-frequency portions of the p/δ_r and r/δ_r frequency responses. Results of this analysis from 0.1 to 1.0 radians per second are plotted in figures 13 (a) and 13 (b) and verify the prediction of a sharp attenuation in amplitude of r/δ_r at a frequency of 0.4 radian per second.

Also shown as dotted lines in figures 13 (b), (c), and (d) are

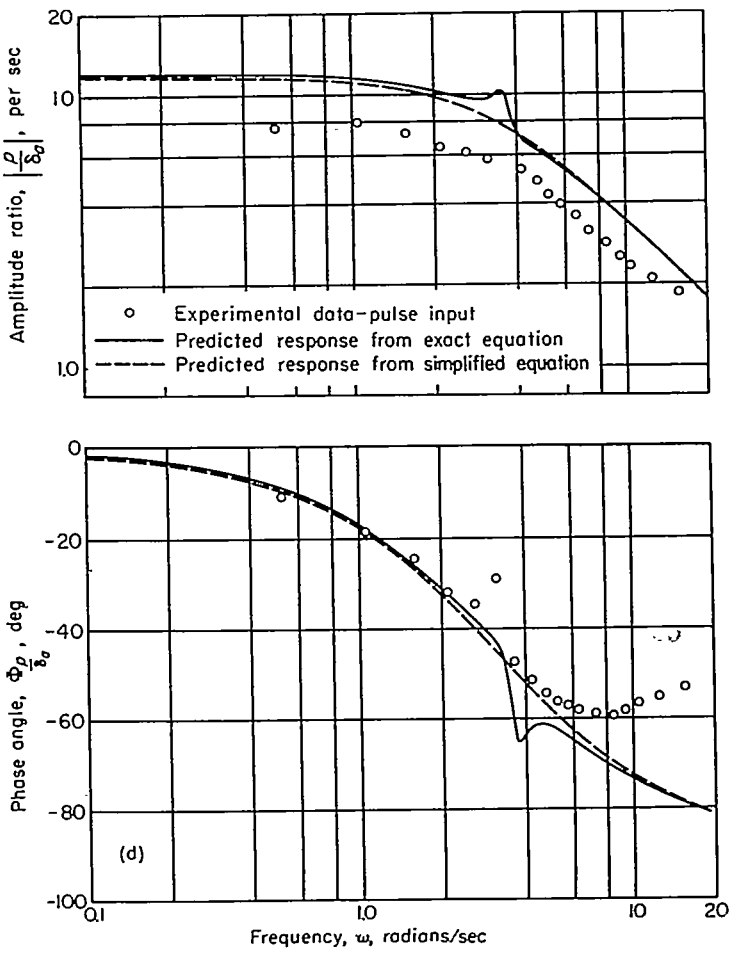

(d) Rolling velocity response to aileron input.

FIGURE 13.—Continued.

responses computed from predicted transfer functions that have been simplified as indicated in the following paragraphs.

THEORETICAL TRANSFER FUNCTIONS

It is shown in Appendix C that the characteristic equation Δ can be factored into the form

$$\Delta = D(D-\lambda_1)(D-\lambda_2)(D^2+c_1D+c_2)$$

where λ_1 and λ_2 are the spiral and rolling roots, respectively, and where c_1 and c_2 are coefficients that define the oscillatory mode. By neglecting λ_1 (which is usually very small) and by omitting other small terms that appear in the numerators of the various response equations, three of the six responses may be reduced to the following simple forms:

$$\left.\begin{aligned} \frac{r}{\delta_r} &= \frac{B_3 D}{D^2+c_1D+c_2} \\ \frac{\beta}{\delta r} &= \frac{-B_3}{D^2+c_1D+c_2} \\ \frac{p}{\delta_a} &= \frac{A_3}{D-\lambda_2} \end{aligned}\right\} \quad (7)$$

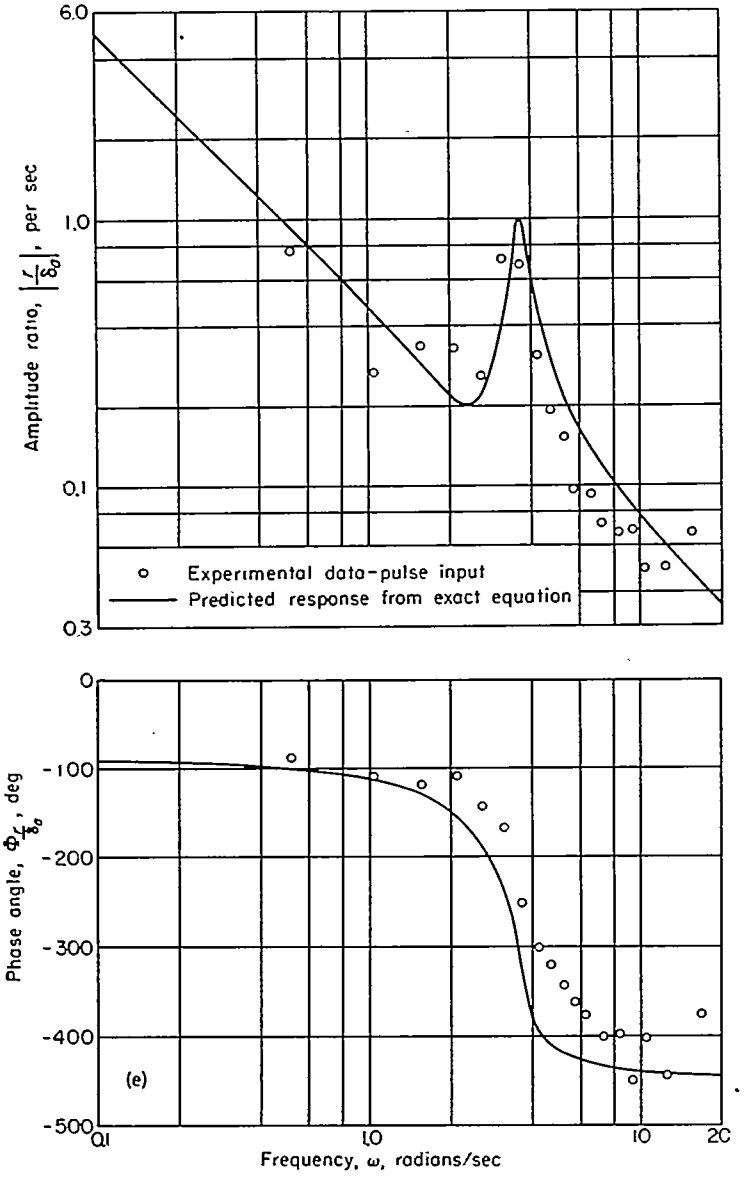

(e) Yawing velocity response to aileron input.

FIGURE 13.—Continued.

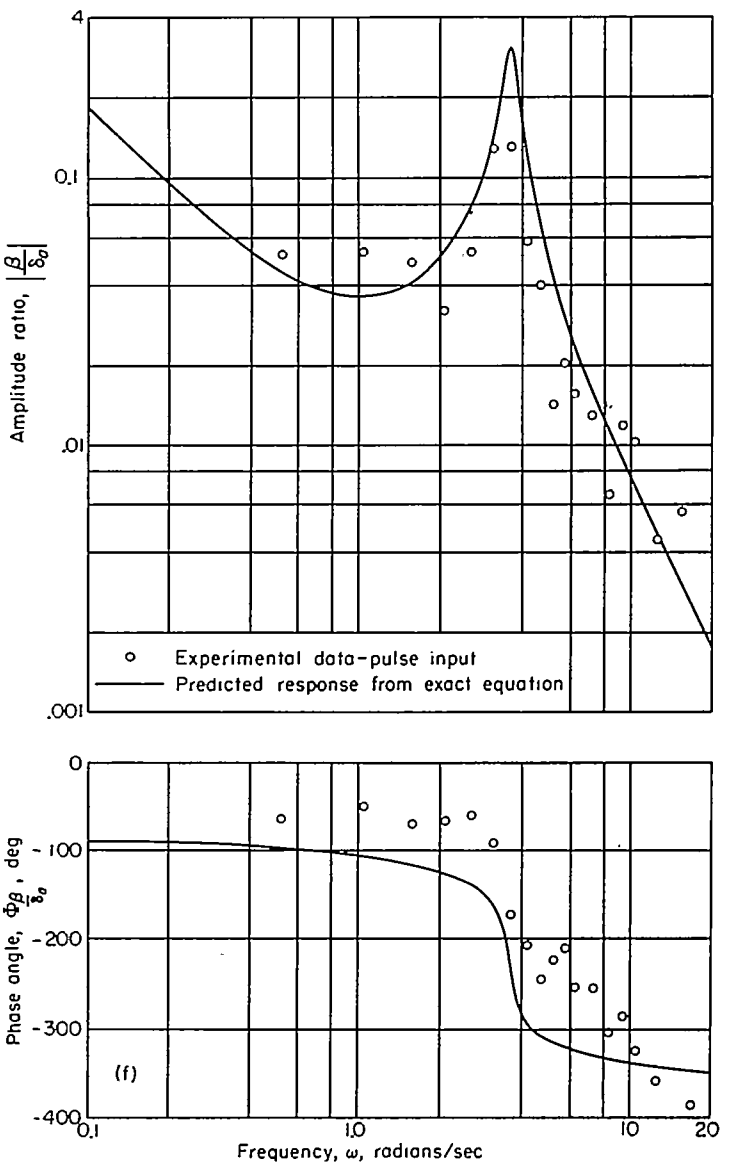

(f) Sideslip angle response to aileron input.

FIGURE 13.—Concluded.

It is also shown that by making additional assumptions as to relative magnitudes, the coefficients λ_3, c_1, and c_2 can be expressed as L_p, $-(N_r+Y_\beta)$, and N_β', respectively. Furthermore, since $B_3 \equiv N_{\delta_r}'$ and $A_3 \equiv L_{\delta_a}'$, equations (7) can be written as

$$\frac{r}{\delta_r}=\frac{N_{\delta_r}'D}{D^2-(N_r+Y_\beta)D+N_\beta'} \tag{8a}$$

$$\frac{\beta}{\delta_r}=\frac{-N_{\delta_r}'}{D^2-(N_r+Y_\beta)D+N_\beta'} \tag{8b}$$

$$\frac{p}{\delta_a}=\frac{L_{\delta_a}'}{D-L_p} \tag{8c}$$

It can be seen that in equations (8a) and (8b) the spiral and rolling modes are completely neglected, and yet, as shown in figures 13 (b) and (c), these simplified transfer functions yield responses that are almost identical to those obtained from the "exact" equations for frequencies greater than 1 radian per second. Similarly, the response computed from equation (8c) closely matches the exact response (fig. 13 (d)) over the frequency range shown except that it omits the small peak normally associated with the oscillatory mode. The spiral mode which has been neglected in all three simple equations appears to have no effect on the calculated airplane response except at frequencies well below 0.1 radian per second.

EXPERIMENTALLY DETERMINED TRANSFER FUNCTIONS

In the analysis of the flight data it was found that the frequency responses of r/δ_r, β/δ_r, and p/δ_a could be successfully simulated by simple transfer functions of the same forms as equations (7). Solutions of these equations on the analog

computer, using final "best" values of the numerical coefficients with actual control motions as recorded in flight, resulted in outputs that closely matched the measured time histories of r, β, and p as shown in figure 3. This fact implies that the modes of motion that are neglected in each case have very little effect on the time response to a pulse-type input.

By use of the coefficients that best describe the measured time histories, frequency responses were calculated for comparison with those derived directly from flight data. Examples of these calculations are shown by the dash-dot lines in figures 13 (b) and (d). These curves, in general, match the experimental points closely for frequencies between 1 and 10 radians per second.

It is apparent from equations (8a) and (8b) that the same information can be obtained from either r/δ_r or β/δ_r. Coefficients evaluated from each of these responses agreed favorably in most cases; however, because of indications that the yaw rate gyro possessed dynamic characteristics superior to those of the sideslip vane, only the yawing velocity responses were used in the final calculations. Natural frequency and damping ratio of this mode are plotted in figure 14.

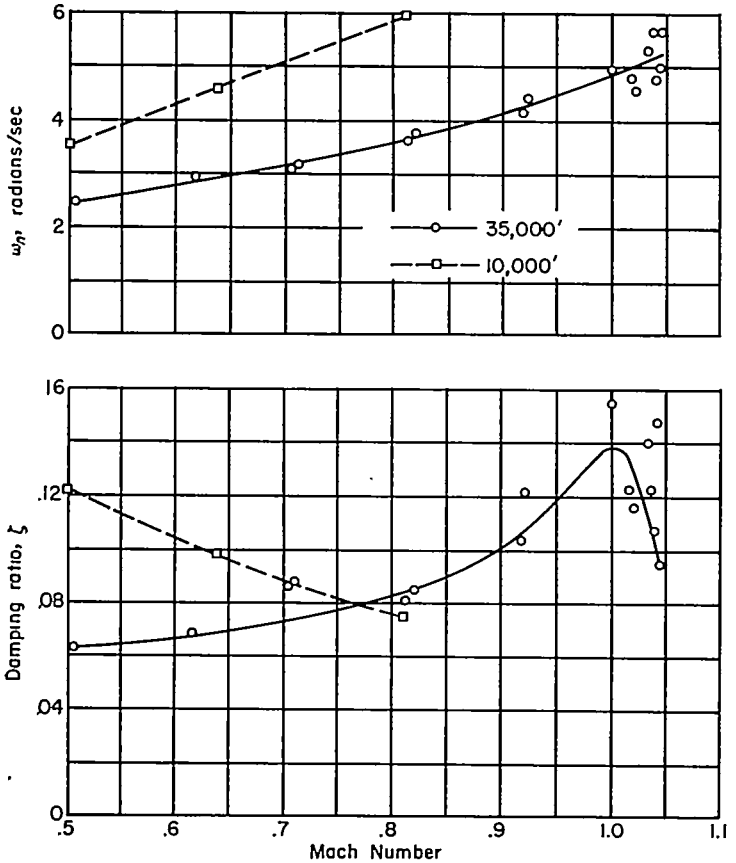

FIGURE 14.—Variation of directional undamped natural frequency and damping ratio with Mach number.

The transfer functions of the three remaining responses p/δ_r, r/δ_a, and β/δ_a were not amenable to simplification. However, it was found that the p/δ_r response could be matched satisfactorily by a transfer function of the type

$$\frac{p}{\delta_r}=\frac{a_1(D+a_2)(D+a_3)}{(D-\lambda_2)(D^2+c_1D+c_2)}$$

which is the same form as developed in Appendix C except that the spiral mode has been neglected. As written here, a_1 is identical to L_{δ_r}' while a_2 and a_3 are complicated combinations of derivatives that cannot be readily simplified. Although this equation closely describes the measured time histories (fig. 3), it was difficult to find unique values of the numerator coefficients. Changes in one of these could be compensated for by corresponding changes in the other two, and the values were not considered to be reliable enough for presentation.

Definition of the r/δ_a and β/δ_a responses required fourth-order transfer functions that include all three modes and, because of practical difficulties involved, no attempt was made to evaluate the coefficients of these responses.

STABILITY DERIVATIVES

In addition to the quantities L_p, N_r+Y_β, N_β', N_{δ_r}', and L_{δ_a}', that were determined as mentioned in the preceding paragraphs, the coefficient L_β' was evaluated from the time histories of rolling and yawing velocity as outlined in Appendix D.

The quantities N_β, L_β, N_{δ_r}, and L_{δ_a} can then be calculated from N_β', L_β', N_{δ_r}', and L_{δ_a}' by using the following expressions obtained from the relationships developed in Appendix C:

$$N_\beta=\frac{N_\beta'-r_ZL_\beta'}{1-r_Xr_Z}$$

$$L_\beta=\frac{L_\beta'-r_XN_\beta'}{1-r_Xr_Z}$$

$$N_{\delta_r}=\frac{N_{\delta_r}'-r_ZL_{\delta_r}'}{1-r_Xr_Z}$$

$$L_{\delta_a}=\frac{L_{\delta_a}'-r_XN_{\delta_a}'}{1-r_Xr_Z}$$

Because r_X and r_Z are very small quantities, wind-tunnel estimates of L_{δ_r}' were assumed to be sufficiently accurate to use in the calculation of N_{δ_r}. The term $r_XN_{\delta_a}'$ was completely neglected in evaluating L_{δ_a}.

Finally, from the definitions given in the notation it is possible to evaluate the derivatives C_{l_p}, C_{n_β}, C_{l_β}, $C_{n_{\delta_r}}$, and $C_{l_{\delta_a}}$.

The analysis methods used herein do not allow the separation of the damping term N_r+Y_β. As compared to N_r, the term Y_β is small and can generally be predicted accurately from wind-tunnel measurements. Therefore values of C_{Y_β} given in table II were used in calculating C_{n_r} from the quantity N_r+Y_β.

The flight evaluated derivatives for both altitudes are plotted against Mach number in figures 15 and 16. These are compared to the predicted values listed in table II. Through the speed range of the test the predictions for both altitudes are essentially the same, except as noted in the plot of C_{l_β}.

The correlation between predicted derivatives and those evaluated from flight at 35,000 feet is generally good except, in some cases, at speeds near a Mach number of 1.0 where the predictions are apt to be inaccurate. Unpredicted variations with altitude are also apparent in the flight values of C_{l_p}, C_{n_r}, and $C_{n_{\delta_r}}$. At a Mach number of 0.8 the value of C_{n_r} for 10,000 feet is less than one half the value at 35,000 feet. Flight data of reference 6 when expressed in this form show a similar trend. The plot of $C_{n_{\delta_r}}$ indicates the same tendency to a lesser degree, while the 10,000-foot value of C_{l_p} (at $M=0.8$) is some 50 percent higher than the value at 35,000 feet. A possible explanation for these discrepancies is that since dynamic pressure varies with altitude, structural deflections due to aerodynamic and inertial loads may cause changes in the effective values of the derivatives.

Values of C_{l_β} determined in the present investigation agree favorably with wind-tunnel results, while those reported in reference 7 (obtained from static flight tests of the same airplane) are much smaller in magnitude. It appears, however, that the results of reference 7 are subject to error because of the simplifying assumptions made. A more rigorous approach would have resulted in larger values of this derivative.

Examination of figure 16 shows the control effectiveness derivatives $C_{n_{\delta_r}}$ and $C_{l_{\delta_a}}$ to have similar variations with increasing Mach number, and in each case the measurecd values are generally smaller than predicted. Values of $C_{l_{\delta_a}}$ obtained in the present investigation agree closely with those presented in reference 8 which again were evaluated from flight measurements of the same airplane.

In this investigation there was no evidence of nonlinear variations of rolling or yawing-moment coefficients with p, r, or β. This was concluded because (1) the period and damping of the oscillations following a control input were essentially constant in every case (no systematic variations with amplitude), and (2) the experimental time histories could be matched, in general, by differential equations with constant coefficients.

No conclusions are drawn as to nonlinear moment coefficient variations with δ_a or δ_r because the magnitudes of the control inputs were not varied appreciably during the tests. They were small enough, however, so that it could be assumed that the linear ranges were not exceeded.

CONCLUDING REMARKS

A flight investigation has been performed on a 35° swept-wing airplane in which the dynamic response characteristics were measured. Transient responses to elevator, rudder, and aileron deflections were recorded through the Mach number range of 0.50 to 1.04. The following remarks can be made regarding the longitudinal and lateral-directional characteristics.

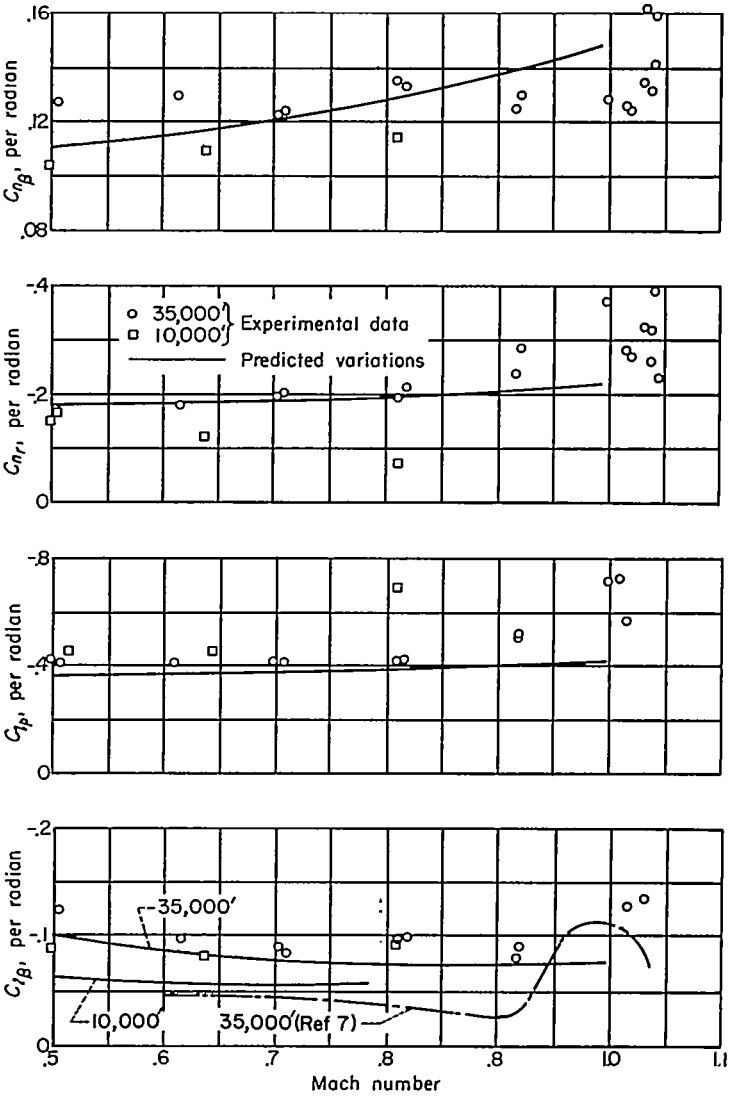

FIGURE 15.—Variation of the derivatives C_{n_β}, C_{n_r}, C_{l_p}, and C_{l_β} with Mach number

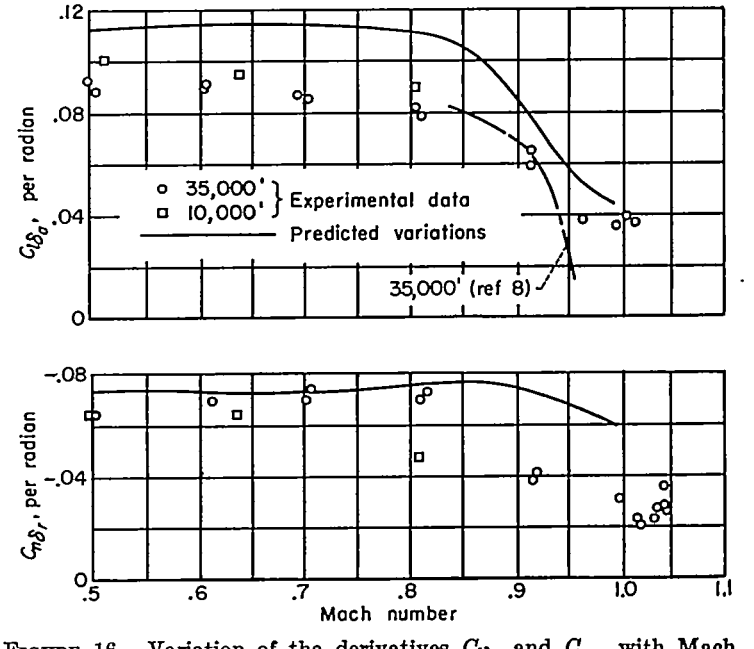

FIGURE 16.—Variation of the derivatives $C_{l_{\delta_a}}$ and $C_{n_{\delta_r}}$ with Mach number.

LONGITUDINAL CHARACTERISTICS

Pitching velocity and normal-acceleration responses could be defined by simple second-order transfer functions as predicted from linear equations of motion. Except for the erratic variation in pitch damping between Mach numbers of 0.90 to 0.95, experimentally determined stability derivatives showed no unusual trends and agreed reasonably well with wind-tunnel predictions.

LATERAL-DIRECTIONAL CHARACTERISTICS

Airplane responses in yawing velocity and sideslip angle due to rudder disturbances were represented by second-order transfer functions that are related solely to the oscillatory mode. Simple first-order equations adequately defined the rolling velocity response to an aileron input. In either case the simplified equations closely defined the measured time histories while describing the frequency responses through the range of 1 to 10 radians per second.

Fourth-order transfer functions calculated from the basic equations of motion using wind-tunnel and theoretical estimates of the various stability derivatives could be simplified by neglecting small quantities and by making approximate cancellations until they were of the same form as those evaluated from flight data. Furthermore, it was possible to express the coefficients of these transfer functions in terms of individual stability derivatives. Frequency responses computed from these simplified equations were almost identical (between 1 and 10 radians per second) to those computed from the exact fourth-order transfer functions, and when compared with experimental results there was generally good agreement. Thus it is concluded that the simplified transfer functions form a reliable basis not only for estimating airplane responses but also for the flight evaluation of stability derivatives, and the methods used here are felt to be sufficiently general to apply to any conventional airplaine.

Experimental values of the derivatives C_{n_β}, C_{l_β}, C_{l_p}, C_{n_r}, $C_{n_{\delta_r}}$, and $C_{l_{\delta_a}}$ compared favorably with predictions, based on theory and wind-tunnel measurements, at Mach numbers below 0.95, while at higher speeds, where predictions are questionable, there was some deviation. There were also notable discrepancies in flight values of C_{l_p} and C_{n_r}, obtained at the 10,000 foot altitude, which were attributed to structural deformations resulting from aerodynamic and inertia loads. Additional evidence of aeroelasticity appeared when the Fourier analysis for p/δ_a was extended to frequencies beyond 10 radians per second; the frequency response showed evidence of aeroelastic deformation which appeared as an additional mode of motion not consistent with rigid airplane theory.

AMES AERONAUTICAL LABORATORY
NATIONAL ADVISORY COMMITTEE FOR AERONAUTICS
MOFFETT FIELD, CALIF., *Sept. 17, 1952*

APPENDIX A

TRANSFER OF AXES

The equations of motion normally used in airplane dynamics are based on a system of axes fixed in the airplane in which the X axis is the intersection of the plane of symmetry and a plane perpendicular to the plane of symmetry that contains the relative wind vector. These are normally referred to as stability axes. The angular displacement between the longitudinal stability axis and the reference axis of the airplane is equal to the trim angle of attack α_T. Since recording instruments are generally alined with the reference axis, measurements of angular rates may be corrected to conform to stability axes notation as indicated in figure 17. Here p and r are vector components of the resultant rotation of the airplane, and the subscript 1 refers to the reference or body axes.

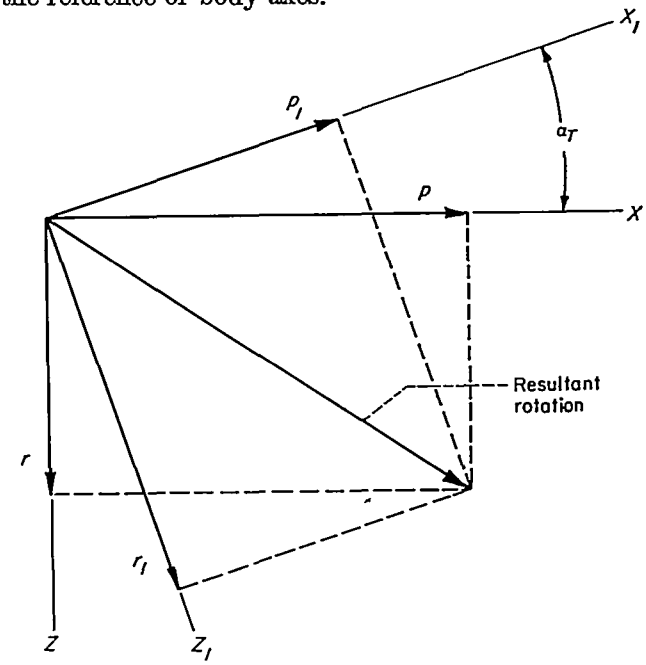

FIGURE 17.—Transfer of axes.

From figure 17 it can be seen that

$$p=p_1 \cos \alpha_T+r_1 \sin \alpha_T$$

$$r=r_1 \cos \alpha_T-p_1 \sin \alpha_T$$

Sideslip angles can be transformed by the relation

$$\tan \beta=\tan \beta_1 \cos \alpha_T$$

For most purposes these conversions are required only when the angle of attack is large. In this investigation it was found that the corrections to rolling velocity could be neglected in all cases because of the high roll to yaw ratio when using either a rudder or aileron input. In the cases of the yawing velocity records, however, the correction was sizable, particularly with the aileron input. The correction to β was neglected in every case.

APPENDIX B

CONTROL INPUTS

When frequency responses are to be calculated from transient records, care should be given to the choice of a suitable forcing function. The frequency range through which accurate transformations can be obtained is definitely limited by the shape of the control input. Theoretically, a pure impulse (zero time duration) is the most desirable input for all purposes because it gives uniform excitation to the entire frequency spectrum. The transform of a step input, on the other hand, has a magnitude that varies inversely with frequency and thus gives infinite excitation to the zero frequency component at the expense of the higher frequencies.

The nearest physical approach to a pure impulse is an input that is roughly triangular in shape as shown in figure 18. Letting a equal the slope and T equal the time base of the triangle, the Fourier transformation of this input can be obtained from the relation

$$\delta(i\omega)=\int_0^T \delta(t)e^{-i\omega t}dt$$

Integration results in a transformation with the following real and imaginary parts:

$$R=\frac{2a}{\omega^2}\cos\frac{\omega T}{2}\left(1-\cos\frac{\omega T}{2}\right) \tag{B1}$$

$$I=\frac{2a}{\omega^2}\sin\frac{\omega T}{2}\left(\cos\frac{\omega T}{2}-1\right) \tag{B2}$$

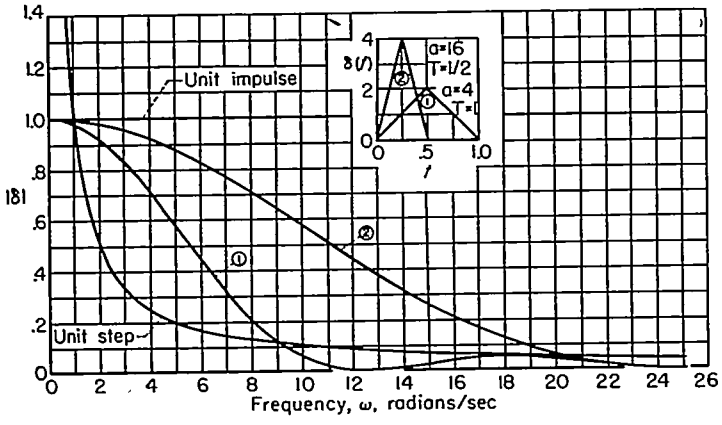

FIGURE 18.—Fourier transform magnitudes of a step, an impulse, and two triangular-shaped inputs.

The magnitude of the transformation is then

$$|\delta|=\frac{2a}{\omega^2}\left(1-\cos\frac{\omega T}{2}\right)$$

It can be seen that $|\delta|$ is periodic and is zero when $\omega=4\pi/T$, $8\pi/T$, ... At these frequencies the transform of the response to this input would also be zero, and thus the ratio of output to input would be indeterminate. A reduction in T would increase the period and reduce the number of indeterminate points. This is shown in figure 18 where the transform magnitudes of two triangular pulses are plotted. One has $T=1$ second and $a=4$, while the other has $T=\frac{1}{4}$ and $a=16$. The areas under the two triangles are equal so that the transforms have equal magnitudes at zero frequency. Reducing T from 1 second to $\frac{1}{4}$ second doubles the period and moves the first indeterminate point from a frequency of 4π radians per second to 8π. For purposes of comparison, transformations of a unit step and a unit impulse are also shown.

As T is further reduced, the magnitude of the triangular pulse more closely approaches the constant value that is characteristic of the pure impulse. To gain full advantage from the smaller T, the slope must be increased to maintain the same area under the pulse. A practical limitation is fixed by the maximum rate at which a control surface can be moved, and any further reduction in T results in smaller over-all magnitudes. The most desirable input, therefore, is a compromise between large area and short time duration.

From figure 18 it would appear that a pulse-type input is well suited for determining low-frequency characteristics. However, the following explanation will show that this is not true.

Generally it is impossible to return a control surface precisely to its initial position after application of a pulse input. Even if a chain stop or other device is used there is still apt to be a small residual deflection $\delta(T)$ after time T.

If $\delta(T)$ is exactly zero, then as ω approaches zero (from eqs. (B1) and (B2))

$$I\to 0$$

$$R\to\frac{aT^2}{4}$$

Now if $\delta(T)$ is finite, the real and imaginary parts of the transform of the entire input are

$$I=\frac{2a}{\omega^2}\sin\frac{\omega T}{2}\left(\cos\frac{\omega T}{2}-1\right)-\frac{\delta(T)}{\omega}\cos\omega T$$

$$R=\frac{2a}{\omega^2}\cos\frac{\omega T}{2}\left(1-\cos\frac{\omega T}{2}\right)-\frac{\delta(T)}{\omega}\sin\omega T$$

In this case as $\omega\to 0$,

$$I\to\infty$$

$$R\to\frac{aT^2}{4}-\delta(T)T$$

thus the zero frequency magnitude is infinitely large regardless of how small $\delta(T)$ may be. Therefore, even though $\delta(T)$ appears to be zero on a flight record (i. e., $\delta(T)$ is less than the least count of the recording instrument), there is still the possibility of an infinite error at zero frequency. A step input is not subject to these large low-frequency errors; an error of 1 percent in the reading of the step deflection merely means an error of 1 percent in the transformation.

APPENDIX C

PREDICTED AIRPLANE RESPONSES

For constant forward velocity and only small disturbances from trimmed flight, the equations that define the motions of an airplane can be divided into two independent groups, the longitudinal equations and the lateral-directional equations. For convenience, these are handled separately in developing theoretical transfer functions.

LONGITUDINAL RESPONSES

In view of the assumptions made, the longitudinal equations may be written as

$$mV(\dot{\alpha}-q)=-q_oS(C_{L_\alpha}\alpha+C_{L_{\delta_e}}\delta_e) \tag{C1}$$

$$I_y\dot{q}=q_oSc(C_{m_\alpha}\alpha+C_{m_{\delta_e}}\delta_e)+\frac{q_oSc^2}{2V}(C_{m_q}q+C_{m_{\dot{\alpha}}}\dot{\alpha}) \tag{C2}$$

Dividing the equation (C1) by mV and (C2) by I_y the equations may be rewritten as

$$\dot{\alpha}-q=Z_\alpha\alpha+Z_{\delta_e}\delta_e \tag{C3}$$

$$\dot{q}=M_\alpha\alpha+M_{\delta e}\delta_e+M_q q+M_{\dot{\alpha}}\dot{\alpha} \tag{C4}$$

Applying the Laplace transformation for zero initial conditions and solving simultaneously for q and α gives

$$\frac{q}{\delta_e}=\frac{C_{1q}D+C_{oq}}{D^2+bD+k} \tag{C5}$$

$$\frac{\alpha}{\delta_e}=\frac{C_{1\alpha}D+C_{o\alpha}}{D^2+bD+k} \tag{C6}$$

where

$$b=-Z_\alpha-M_q-M_{\dot{\alpha}} \tag{C7}$$

$$k=Z_\alpha M_q-M_\alpha \tag{C8}$$

$$C_{1q}=M_{\delta_e}+Z_{\delta_e}M_{\dot{\alpha}} \tag{C9}$$

$$C_{oq}=M_\alpha Z_{\delta_e}-M_{\delta_e}Z_\alpha \tag{C10}$$

$$C_{1\alpha}=Z_{\delta_e} \tag{C11}$$

$$C_{o\alpha}=M_{\delta_e}-Z_{\delta_e}M_q \tag{C12}$$

The incremental change in normal acceleration is defined as $n=V(\dot{\alpha}-q)$.
Thus

$$\frac{n}{\delta_e}=V\left(D\frac{\alpha}{\delta_e}-\frac{q}{\delta_e}\right)$$

$$=\frac{C_{2n}D^2+C_{1n}D+C_{on}}{D^2+bD+k} \tag{C13}$$

where

$$C_{2n}=VZ_{\delta_e} \tag{C14}$$

$$C_{1n}=-VZ_{\delta_e}(M_q+M_\alpha) \tag{C15}$$

$$C_{on}=-V(M_\alpha Z_{\delta_e}-M_{\delta_e}Z_\alpha)=-VC_{oq} \tag{C16}$$

In most conventional aircraft C_{2n} and C_{1n} are very small compared to C_{on} and thus

$$\frac{n}{\delta_e}\approx\frac{C_{on}}{D^2+bD+k}$$

The stability derivatives C_{m_α}, $C_{m_q}+C_{m_{\dot{\alpha}}}$, and $C_{m_{\delta_e}}$ may be obtained from approximate expressions for the transfer-function coefficients.

The term C_{m_α} can be determined from k (eq. (C8)) by omitting the term $Z_\alpha M_q$. Investigation has shown that, in this case, this term is very small compared to M_α. Thus

$$k=-M_\alpha=-C_{m_\alpha}\frac{q_oSc}{I_y}$$

or

$$C_{m_\alpha}=-\frac{kI_y}{q_oSc} \tag{C17}$$

The damping factor $C_{m_q}+C_{m_{\dot{\alpha}}}$ can be obtained from equation (C7) by using known values of b and C_{L_α}.

$$M_q+M_{\dot{\alpha}}=-Z_\alpha-b$$

or

$$C_{m_q}+C_{m_{\dot{\alpha}}}=\frac{2VI_y}{q_oSc^2}\left(C_{L_\alpha}\frac{q_oS}{mV}-b\right) \tag{C18}$$

The elevator effectiveness derivative $C_{m_{\delta_e}}$ can be determined from equation (C9). The term $Z_{\delta_e}M_{\dot{\alpha}}$ is, for conventional aircraft, very small as compared with M_{δ_e}, and thus

$$M_{\delta_e}=C_{1q}$$

or

$$C_{m_{\delta_e}}=\frac{Iy}{q_oSc}C_{1q} \tag{C19}$$

LATERAL-DIRECTIONAL RESPONSES

Equations of motion.—The three equations that define the lateral and directional motions of the airplane may be written as:

$$\left(I_XD^2-q_oSb\,C_{l_p}\frac{b}{2V}D\right)\varphi+\left(-I_{XZ}D^2-q_oSb\,C_{l_r}\frac{b}{2V}D\right)\psi-$$

$$q_oSb\,C_{l_\beta}\beta=q_oSb\,C_{l_\delta}\delta \tag{C20}$$

$$\left(-I_{XZ}D^2-q_oSb\,C_{n_p}\frac{b}{2V}D\right)\varphi+\left(I_ZD^2-q_oSb\,C_{n_r}\frac{b}{2V}D\right)\psi-$$

$$q_oSb\,C_{n_\beta}\beta=q_oSb\,C_{n_\delta}\delta \tag{C21}$$

$$(-W\cos\gamma)\varphi+(mVD-W\sin\gamma)\psi+$$

$$(mVD-q_oSC_{Y_\beta})\beta=q_oSC_{Y_\delta}\delta \tag{C22}$$

By dividing equation (C20) by I_X, equation (C21) by I_Z, equation (C22) by mV, and by introducing new symbols, the three equations become:

$$(D^2-L_pD)\varphi+(-r_XD^2-L_rD)\psi-L_\beta\beta=L_\delta\delta \tag{C23}$$

$$(-r_ZD^2-N_pD)\varphi+(D^2-N_rD)\psi-N_\beta\beta=N_\delta\delta \tag{C24}$$

$$-K_1\varphi+(D-K_2)\psi+(D-Y_\beta)\beta=Y_\delta\delta \tag{C25}$$

CHARACTERISTIC EQUATION

The characteristic equation Δ is formed by expanding the major determinant to give

$$\Delta=D(C_4D^4+C_3D^3+C_2D^2+C_1D+C_o) \qquad \text{(C26)}$$

where

$C_4=1-r_Xr_Z$

$C_3=-L_p-N_r-Y_\beta(1-r_Xr_Z)-r_XN_p-r_ZL_r$

$C_2=(N_r+r_ZL_r)Y_\beta+(L_p+r_XN_p)Y_\beta+(L_pN_r-N_pL_r)+(N_\beta+r_ZL_\beta)$

$C_1=-(L_pN_r-N_pL_r)Y_\beta+(L_\beta N_p-N_\beta L_p)-K_1(L_\beta+r_XN_\beta)-K_2(N_\beta+r_ZL_\beta)$

$C_o=-K_1(L_rN_\beta-N_rL_\beta)-K_2(L_\beta N_p-N_\beta L_p)$

These coefficients can be further simplified by making the following substitutions:

Let

$$L_p'=L_p+r_XN_p \qquad N_r'=N_r+r_ZL_r$$

$$L_\beta'=L_\beta+r_XN_\beta \qquad N_\beta'=N_\beta+r_ZL_\beta$$

Then the coefficients of the characteristic equation are finally expressed as

$C_4=1-r_Xr_Z$

$C_3=L_p'-N_r'-Y_\beta(1-r_Xr_Z)$

$C_2=(N_r'+L_p')Y_\beta+(L_pN_r-N_pL_r)+N_\beta'$

$C_1=-(L_pN_r-N_pL_r)Y_\beta+(L_\beta N_p-N_\beta L_p)-K_1L_\beta'-K_2N_\beta'$

$C_o=-K_1(L_rN_\beta-N_rL_\beta)-K_2(L_\beta N_p-N_\beta L_p)$

In factored form, equation (C26) is

$$\Delta=D(D-\lambda_1)(D-\lambda_2)(D-\lambda_3)(D-\lambda_4)$$

where λ_1 and λ_2 are designated as the spiral and rolling roots, respectively, and where λ_3 and λ_4 are a complex pair $(\sigma\pm i\omega_1)$ that describe the oscillatory mode.

For convenience in this investigation Δ has been expressed as

$$\Delta=D(D-\lambda_1)(D-\lambda_2)(D^2+c_1D+c_2)$$

where

$$c_1=-(\lambda_3+\lambda_4)=-2\sigma$$

$$c_2=\lambda_3\lambda_4=\sigma^2+\omega_1^2$$

Here c_1 and c_2 are real coefficients that define the damping and period of the oscillatory motion.

The quadratic term may also be written in the form

$$\omega_n^2\left(1+2\zeta\frac{D}{\omega_n}+\frac{D^2}{\omega_n^2}\right)$$

where

$$\omega_n=\sqrt{c_2}$$

and

$$\zeta=\frac{c_1}{2\omega_n}$$

SIMPLIFICATIONS OF THE CHARACTERISTIC EQUATION

If C_o and other small terms are neglected when the flight-path angle γ and when the product of inertia are essentially zero, the characteristic equation may be written as

$$\Delta=D^2[D^3-(L_p+N_r+Y_\beta)D^2+(L_pY_\beta+L_pN_r+N_\beta)D-L_pN_\beta]$$

The cubic term can be factored exactly so that

$$\Delta=D^2(D-L_p)[D^2-(N_r+Y_\beta)D+N_\beta]$$

This form of the characteristic equation considers only the oscillatory and rolling modes. It enables the coefficients C_1, C_2, and C_3 to be expressed directly in terms of aerodynamic derivatives or simple combinations thereof.

Even when the product of inertia is significant, the characteristic equation may be factored approximately into the simple form

$$\Delta=D^2(D-L_p)[D^2-(N_r+Y_\beta)D+N_\beta']$$

While the factorization is not exact, it is nevertheless justifiable in many cases.

TRANSFER FUNCTIONS

From the three equations of motion the airplane responses in φ, ψ, and β can be readily calculated. In the following equations, δ refers to either an aileron or a rudder disturbance.

$$\frac{\varphi}{\delta}=\frac{A_3D^3+A_2D^2+A_1D+A_0}{\Delta}$$

where

$A_3=L_\delta+r_XN_\delta$

$A_2=-L_\delta(Y_\beta+N_r)+N_\delta(L_r-r_XY_\beta)+Y_\delta L_\beta'$

$A_1=L_\delta(N_rY_\beta+N_\beta)-N_\delta(L_\beta+L_rY_\beta)+Y_\delta(L_rN_\beta-N_rL_\beta)$

$A_o=K_2(N_\delta L_\beta-N_\beta L_\delta)$

$$\frac{\psi}{\delta}=\frac{B_3D^3+B_2D^2+B_1D+B_0}{\Delta}$$

where

$B_3=N_\delta+r_ZL_\delta$

$B_2=-N_\delta(L_p+Y_\beta)+L_\delta(N_p-r_ZY_\beta)+Y_\delta N_\beta'$

$B_1=N_\delta L_pY_\beta-L_\delta N_pY_\beta+Y_\delta(L_\beta N_p-N_\beta L_p)$

$B_o=K_1(L_\delta N_\beta-N_\delta L_\beta)$

$$\frac{\beta}{\delta}=\frac{D(E_3D^3+E_2D^2+E_1D+E_o)}{\Delta}$$

where

$E_3=Y_\delta(1-r_Xr_Z)$

$E_2=-Y_\delta(N_r'+L_p')-L_\delta r_Z-N_\delta$

$E_1=Y_\delta(L_pN_r-N_pL_r)-L_\delta(N_p-r_ZK_2-K_1)+N_\delta(r_XK_1+L_p+K_2)$

$E_o=K_1(N_\delta L_r-L_\delta N_r)+K_2(L_\delta N_p-N_\delta L_p)$

Simplifications can also be made in these expressions by neglecting small quantities; however, this can be shown more clearly in the numerical example that follows.

NUMERICAL EXAMPLE AT $M=0.8$

By use of values of stability derivatives shown in table II, and with $\gamma=0$, predicted responses for $p=D\varphi$, $r=D\psi$, and β

for both aileron and rudder inputs have been calculated and found to be

$$\Delta = D(D^4+3.652D^3+15.16D^2+41.26D+0.0289)$$

$$= D(D+0.00070)\ (D+3.078)\ (D^2+0.573D+13.40)$$

$$\frac{r}{\delta_r} = \frac{-7.60D(D+3.091)(D^2+0.0270D+0.208)}{\Delta}$$

$$\frac{p}{\delta_r} = \frac{5.16D^2(D+4.436)(D-5.210)}{\Delta}$$

$$\frac{\beta}{\delta_r} = \frac{0.0339D(D+3.053)(D+225.3)(D-0.00703)}{\Delta}$$

$$\frac{r}{\delta_a} = \frac{0.699D(D+3.978)(D^2-1.758D+7.358)}{\Delta}$$

$$\frac{p}{\delta_a} = \frac{36.4D^2(D^2+0.655D+13.68)}{\Delta}$$

$$\frac{\beta}{\delta_a} = \frac{0.0008D(D+0.990)(D-1.094)(D-870)}{\Delta}$$

When small terms are neglected, r/δ_r can be expressed as

$$\frac{r}{\delta_r} = \frac{-7.60D^3(D+3.091)}{D^2(D+3.078)(D^2+0.573D+13.40)}$$

and then by an approximate cancellation this reduces to

$$\frac{r}{\delta_r} = \frac{-7.60D}{D^2+0.573D+13.40}$$

Similarly, β/δ_r can be simplified by neglecting small terms so that

$$\frac{\beta}{\delta_r} = \frac{7.64D^2(D+3.053)}{D^2(D+3.078)(D^2+0.573D+13.40)} \approx \frac{7.64}{D^2+0.573D+13.40}$$

It can be seen that this expression for β/δ_r is practically identical (with opposite sign) to the integral of the simplified equation for r/δ_r. It is also possible to simplify p/δ_a as follows:

$$\frac{p}{\delta_a} = \frac{36.4D^2(D^2+0.655D+13.68)}{D^2(D+3.078)(D^2+0.573D+13.40)} \approx \frac{36.4}{D+3.078}$$

Similar simplifications have been made for other Mach numbers and found to be equally valid.

APPENDIX D

FLIGHT EVALUATION OF C_{l_β}

From time histories of the free oscillatory responses of p and r, it is possible to evaluate the derivative C_{l_β} as follows. If the rolling moment and yawing moment equations (C23) and (C24) are set equal to zero, then the ratio $\frac{\varphi}{\psi}$ of the free oscillation may be obtained by simultaneous solution of the two equations to give

$$\frac{\varphi}{\psi} = \frac{(r_X D^2+L_r D)N_\beta+(D^2-N_r D)L_\beta}{(D^2-L_p D)N_\beta+(r_Z D^2+N_p D)L_\beta}$$

or

$$\frac{\varphi}{\psi} = \frac{L_\beta' D+L_r N_\beta-N_r L_\beta}{N_\beta' D-L_p N_\beta+N_p L_\beta}$$

The quantity $L_r N_\beta - N_r L_\beta$ in the numerator is generally very small and can be neglected. In the denominator, the term $N_p L_\beta$ is small compared to the other terms and can also be neglected. The ratio, $\frac{\varphi}{\psi}$, is then simplified to

$$\frac{\varphi}{\psi} = \frac{L_\beta' D}{N_\beta'(D-L_p)}$$

When the complex root $\lambda_3 = \sigma + i\omega_1$ is substituted for the operator D, this expression is the ratio of the free oscillatory responses of φ and ψ at any time t. The ratio of p to r is obviously the same and can be expressed as

$$\frac{p}{r} = \frac{L_\beta'(\sigma+i\omega_1)}{N_\beta'(\sigma+i\omega_1-L_p)}$$

The actual magnitude of this ratio is

$$\left|\frac{p}{r}\right| = \frac{L_\beta'\sqrt{\sigma^2+\omega_1^2}}{N_\beta'\sqrt{(\sigma-L_p)^2+\omega_1^2}}$$

In this form $|p/r|$ is the ratio at any time t of the amplitudes of the envelopes that enclose the oscillatory motions of p and r; σ is the rate of damping of the envelope; and ω_1 is the natural frequency of oscillation. When σ is very small as compared to ω_1 it can be omitted; thus

$$\left|\frac{p}{r}\right| = \frac{L_\beta'\omega_1}{N_\beta'\sqrt{L_p^2+\omega_1^2}} = \frac{L_\beta'}{N_\beta'\sqrt{1+(L_p/\omega_1)^2}}$$

If N_β' and L_p are known, it is then possible to evaluate L_β' from measured time histories of p and r.

REFERENCES

1. Thompson, Jim Rogers, Bray, Richard S., and Cooper, George E.: Flight Calibration of Four Airspeed Systems on a Swept-Wing Airplane at Mach Numbers up to 1.04 by the NACA Radar-Phototheodolite Method. NACA RM A50H24, 1950.
2. Gardner, Murray F., and Barnes, John L.: Transients in Linear Systems Studied by the Laplace Transformation, vol. 1. John Wiley & Sons, Inc., N. Y., 1942.
3. Draper, Charles S., McKay, Walter, and Lees, Sidney: Instrument Engineering. Vol. 2, Methods for Associating Mathematical Solutions With Common Forms. McGraw Hill Book Co., N. Y., 1953.
4. Brown, Gordon S., and Campbell, Donald P.: Principles of Servomechanisms. John Wiley & Sons, Inc., N. Y., 1948.
5. Morrill, Charles P., Jr., and Boddy, Lee E.: High-Speed Stability and Control Characteristics of a Fighter Airplane Model With a Swept-Back Wing and Tail. NACA RM A7K28, 1948.
6. McNeill, Walter E., and Cooper, George E.: A Comparison of the Measured and Predicted Lateral Oscillatory Characteristics of a 35° Swept-Wing Fighter Airplane. NACA RM A51C28, 1951.
7. Rathert, George A., Jr., Rolls, L. Stewart, Winograd, Lee, and Cooper, George E.: Preliminary Flight Investigation of the Wing-Dropping Tendency and Lateral-Control Characteristics of a 35° Swept-Wing Airplane at Transonic Mach Numbers. NACA RM A50H03, 1950.
8. McFadden, Norman M., Rathert, George A., Jr., and Bray, Richard S.: The Effectiveness of Wing Vortex Generators in Improving the Maneuvering Characteristics of a Swept-Wing Airplane at Transonic Speeds. NACA RM A51J18, 1952.

TABLE I.—PHYSICAL CHARACTERISTICS OF TEST AIRPLANE

Wing	
Total area	287.9 sq ft
Span	37.1 ft
Aspect ratio	4.79
Taper ratio	0.51
Mean aerodynamic chord	97.03 in.
Dihedral	3°
Sweepback of quarter-chord line	35°14′
Aerodynamic and geometric twist	2°
Root airfoil section (normal to quarter-chord line).	NACA 0012–64 (modified)
Tip airfoil section (normal to quarter-chord line)	NACA 0011–64 (modified)
Ailerons	
Area, each	18.6 sq ft
Span	9.18 ft
Chord, average	2.03 ft
Deflection, maximum	14° up, 14° down
Inboard end at	51.6 percent $b/2$
Horizontal tail	
Total area (including 1.20 sq ft covered by fuselage).	35.0 sq ft
Span	12.8 ft
Aspect ratio	4.65
Taper ratio	0.45
Main aerodynamic chord	34.7 in.
Sweepback of 0.25 chord line	34°35′
Airfoil section	NACA 0010–64
Tail length	18.12 ft
Vertical tail	
Area, total	34.4 sq ft
Span	7.5 ft
Aspect ratio	1.74
Taper ratio	0.36
Sweepback of quarter-chord line	35°00′
Rudder	
Area	8.1 sq ft
Span	6.6 ft
Chord, average	1.23 ft
Deflection, maximum	24.8° right, 25° left
Take-off weight (c. g. at 23.0 percent MAC)	14,102 lb
Landing weight (c. g. at 21.9 percent MAC)	11,612 lb
Average weight for calculations (c. g. at 22.5 percent MAC).	12,800 lb
Moment of inertia about X axis	7,245 slug ft^2
Moment of inertia about Y axis	17,480 slug ft^2
Moment of inertia about Z axis	23,190 slug ft^2
Inclination of principal longitudinal axis with respect to fuselage reference axis.	−2.5°

TABLE II.—PARAMETERS USED IN ESTIMATING AIRPLANE RESPONSES

Altitude, 35,000 feet						
M	0.5	0.6	0.7	0.8	0.9	1.0
V	486	583	681	778	875	972
q_o	87.0	125.2	170.6	222.5	281.8	347.5
C_L	.51	.36	.26	.16	.13	.12
α_T	7.2	5.3	3.8	2.8	2.4	1.2
I_{XZ}	−1297	−773	−359	−83	28	336
C_{L_α}	4.15	4.30	4.54	4.93	5.40	4.52
C_{m_α}	−.405	−.455	−.514	−.583	−.990	------
$C_{m_{\dot{\alpha}}}$	−.397	−.395	−.392	−.384	−.260	------
$C_{m_q}+C_{m_{\dot{\alpha}}}$	−6.10	−6.20	−6.32	−6.67	−6.55	------
C_{l_β}	−.1025	−.0857	−.0773	−.0741	−.0721	−.0768
C_{n_β}	.1100	.1146	.1199	.1273	.1366	.1467
C_{Y_β}	−.690	−.701	−.715	−.733	−.757	−.782
C_{l_p}	−.360	−.367	−.375	−.385	−.399	−.414
C_{n_p}	−.0328	−.0225	−.0160	−.0120	−.0092	−.0068
C_{l_r}	.157	.130	.116	.108	.106	.104
C_{n_r}	−.1820	−.1852	−.1896	−.1970	−.2065	−.2170
$C_{l_{\delta_r}}$	.0077	.0102	.0138	.0155	.0160	.0183
$C_{n_{\delta_r}}$	−.0730	−.0728	−.0725	−.0742	−.0736	−.0582
$C_{Y_{\delta_r}}$	.160	.160	.160	.160	.160	.160
$C_{l_{\delta_a}}$	.112	.114	.113	.111	.088	.043
$C_{n_{\delta_a}}$	−.0050	.0020	.0059	.0081	.0095	.0105
$C_{Y_{\delta_a}}$	.004	.004	.004	.004	.004	.004
λ_1	−.00192	−.00113	−.00076	−.00070	−.00027	−.00077
λ_2	−1.809	−2.203	−2.667	−3.078	−3.581	−4.168
c_1	.378	.438	.497	.573	.679	.740
c_2	5.24	7.25	9.91	13.40	18.03	23.45